

# Preservation of Fe isotope heterogeneities during diagenesis and metamorphism of banded iron formation

C. D. Frost · F. von Blanckenburg ·  
R. Schoenberg · B. R. Frost · S. M. Swapp

Received: 22 March 2006 / Accepted: 21 August 2006 / Published online: 28 October 2006  
© Springer-Verlag 2006

**Abstract** We present the iron isotope composition of primary, diagenetic and metamorphic minerals in five samples from the contact metamorphosed Biwabik Iron Formation. These samples attained peak metamorphic temperatures of <200, <340, ~500, <550, and <740°C respectively.  $\delta^{56}\text{Fe}$  of bulk layers ranges from -0.8 to +0.8‰; in some samples the layers may differ by >1‰ on the millimeter scale. Minerals in the lowest grade samples consistently show a sequence in which  $\delta^{56}\text{Fe}$  of magnetite > silicate  $\geq$  carbonate. The inter-mineral Fe isotope differences vary in a fashion that cannot be reconciled with theoretical temperature-dependent fractionation factors. Textural evidence reveals that most, if not all, magnetite in the Biwabik Formation is diagenetic, not primary, and that there was tremendous element mobility during diagenesis. The short duration of contact metamorphism allowed diagenetic magnetite compositions to be preserved throughout prograde metamorphism until at least the appearance of olivine. Magnetite compositions therefore act as an isotope record of the environment in which these sediments formed. Larger-scale fluid flow and longer timescales may allow equilibration of Fe isotopes in regionally metamorphosed rocks to lower

temperatures than in contact metamorphic environments, but weakly regionally metamorphosed rocks may preserve small-scale Fe isotopic heterogeneities like those observed in the Biwabik Iron Formation. Importantly, Fe isotope compositions that are characteristic of chemical sedimentation or hydrothermal processes are preserved at low grade in the form of large inter-mineral variations, and at high grade in the form of unique bulk rock compositions. This observation confirms earlier work that has suggested that Fe isotopes can be used to identify sedimentary processes in the Precambrian rock record.

## Introduction

Igneous and metamorphosed igneous rocks exhibit only small variations in Fe isotopic compositions (Zhu et al. 2002; Beard et al. 2003; Poitrasson et al. 2004; Williams et al. 2004, Poitrasson and Freydieier 2005; Weyer et al. 2005).  $\delta^{56}\text{Fe}$  in basaltic and granitic rocks ranges from ca. 0 to 0.15‰ (expressed relative to the international Fe standard, IRMM-014, throughout this paper) and up to 0.39‰ for high-silica granitoids, accounted for by Fe isotope fractionation during exsolution of late magmatic aqueous fluids from granitic melts (Poitrasson and Freydieier 2005). There is no detectable isotopic fractionation between silicate minerals and magnetite in intermediate composition volcanic rocks (Beard and Johnson 2004), although recent, high-precision measurements suggest that minute intra-mineral and intra-rock fractionations do exist (Poitrasson and Freydieier 2005; Schoenberg et al. 2005; Schuessler et al. 2005).

---

Communicated by F. Poitrasson.

---

C. D. Frost (✉) · B. R. Frost · S. M. Swapp  
Department of Geology and Geophysics,  
University of Wyoming, Laramie, WY 82071, USA  
e-mail: frost@uwo.edu

F. von Blanckenburg · R. Schoenberg  
Institut für Mineralogie, Universität Hannover,  
Callinstrasse 3, 30167 Hannover, Germany

The Fe isotopic compositions of hydrothermal ores and sedimentary rocks are more variable than those of igneous rocks and minerals.  $\delta^{56}\text{Fe}$  of hematite, siderite and sulfide hydrothermal ores vary from  $-2.3$  to  $+1.3\text{‰}$  and are strongly dependent upon fluid and precipitation histories (Graham et al. 2004; Markl et al. 2006). Organic-rich black shales (Yamaguchi et al. 2005; Matthews et al. 2004) define a wide range of  $^{56}\text{Fe}/^{54}\text{Fe}$  isotopic compositions, from  $-2.2$  to  $0.7\text{‰}$ , whereas Fe–Mn crusts (Zhu et al. 2000; Chu et al. 2003) exhibit a range in  $^{56}\text{Fe}/^{54}\text{Fe}$  from  $-0.9$  to  $0.1\text{‰}$ . However, the largest known variations in  $^{56}\text{Fe}/^{54}\text{Fe}$  are exhibited by Precambrian banded iron formations (BIF), which range from  $-2.3\text{‰}$  for pyrite-rich BIF layers to  $1.3\text{‰}$  for magnetite-rich BIF layers (Johnson et al. 2003).

Fe isotopic studies of metasedimentary rocks and minerals are extremely limited. Dauphas et al. (2004) reported Fe isotopic data for amphibolite- and granulite-facies metasedimentary rocks from southwest Greenland. They observed no differences in Fe isotopic composition between bulk rock samples and pyroxene and magnetite mineral separates and concluded that any original inter-mineral variations in Fe isotopic composition were obliterated by high-temperature equilibration during metamorphism. However, the heavy bulk rock Fe isotope compositions of these Early Archean rocks appeared to suggest that they originate from a sedimentary, rather than a meta-igneous environment.

To better understand the behavior of Fe isotopes during diagenesis and metamorphism of metasedimentary rocks, we have undertaken a systematic study of the inter-mineral partitioning of Fe isotopes during progressive contact metamorphism. We have

chosen to study a suite of contact metamorphosed iron-formation samples for two reasons. First, iron formation has a simple chemical composition, rich in Si and Fe with smaller amounts of Mg, Ca and Mn and essentially no Al, Ti, Na and K. This protolith results in metamorphic silicates closely approaching Fe-end member compositions. Consequently their Fe isotopic compositions can be more readily compared to theoretical predictions of their behavior than can be done with minerals of more complex composition. Second, the least metamorphosed portions of the iron formation chosen for study exhibit extreme heterogeneity in Fe isotope composition. A heterogeneous starting material is important for assessing whether Fe-isotopes are homogenized during metamorphism, and allows us to characterize the changes in Fe isotopic composition that accompany mineral reactions occurring during diagenesis and progressive metamorphism.

### Geology of the Biwabik Iron Formation

The Biwabik Formation extends for 190 km across northern Minnesota. It is separated from the correlative, 1.9 Ga Gunflint Formation of Ontario (Fralick et al. 2002) by the intrusion of the 1.1 Ga Duluth gabbro, which developed a spectacular contact aureole within these iron formations (Fig. 1; Gundersen and Schwartz 1962; French 1968; Bonnicheson 1969, 1975; Morey et al. 1972; Morey 1992; Simmons et al. 1974; Floran and Papike 1975, 1978). Both the Biwabik and Gunflint formations lie north of the  $\sim 1.8$  Ga Penokean orogen and had undergone only very low-grade burial

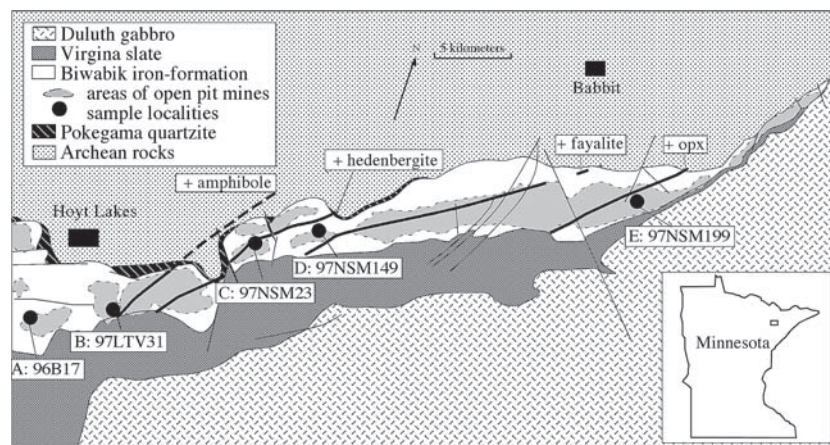


**Fig. 1** Geological sketch map of the portion of the Biwabik Formation from which samples were collected. *Thick lines* delineate contact metamorphic isograds. The pigeonite-in isograd lies immediately adjacent to the easternmost contact of the

Biwabik against the Duluth gabbro in a zone too narrow to be shown in Fig. 1. Samples A and B are from LTV open pit mines; samples C, D, and E are from Northshore Mining Company mines

metamorphism prior to contact metamorphism by the Duluth gabbro. The lowest-grade rocks in the Biwabik Formation are composed of fine-grained quartz, magnetite, siderite, greenalite, and locally, hematite and minnesotaite. Layering occurs on the scale of millimeter to a few centimeter. Rarely, massive greenalite is preserved. More commonly, greenalite-bearing layers consist of sand-size greenalite granules in a chert cement, and are interpreted as having formed as greenalite sand deposited near wave-base (cf. Lanier 1989). Siderite-rich layers typically are homogeneous and fine-grained but locally they contain rip-up clasts and carbonate pisoliths suggesting deposition in a high-energy environment. Exceptionally well-preserved, morphologically diverse, microfossil assemblages have been described from the Gunflint Iron Formation (Barghoorn and Tyler 1965; Knoll et al. 1978; Lanier 1989). The ultra-fine-grained magnetite from stromatolitic chert of the Gunflint Iron-Formation was interpreted by Chang et al. (1989) as biogenic. These studies, among others, suggest that the Biwabik Iron Formation was deposited in a shallow water environment that supported microbial communities.

In the contact metamorphosed portion of the Biwabik Iron Formation, well-exposed in the LTV and Northshore Mining Company mines, we have been able to identify isograds marked by the appearance of the following minerals: (1) grunerite, (2) hedenbergite, (3) olivine, and (4) orthopyroxene (Fig. 1). This study focuses on a suite of five samples representing varying metamorphic grade, from outside the contact aureole to above the fayalite-in isograd.

### Sample descriptions

All samples were collected from fresh faces of active mines, and are unweathered. Because of the finely banded nature of the formation and incomplete exposure across the aureole it was not possible to sample a single horizon with increasing metamorphic grade, therefore there may be variation in the chemical composition of the protoliths. However, the Biwabik Formation is remarkably free of continental detritus (Gundersen and Schwartz 1962); all samples therefore represent chemical metasedimentary rocks. The five samples were chosen to represent a suite that attained a range of peak temperatures from <200 to >700°C as discussed below.

The lowest grade sample, A, lies outside the contact aureole (Fig. 1). It is composed of layers of massive greenalite from 0.1 to 0.5 cm wide, which could consist of compressed greenalite granules, coarse-grained

carbonate-rich layers in which carbonate appears to have partially replaced greenalite granules, and fine-grained carbonate layers that contain sparse greenalite granules (marked “G” on Fig. 2a). The abundance of magnetite is variable. Little to no magnetite is present in the thicker, fine-grained carbonate-rich layer (marked “S” on Fig. 2a) but fine-grained magnetite (<0.1 mm) is present in the adjacent thin fine-grained carbonate-rich one. Idioblastic magnetite also forms rims on greenalite granules and has replaced greenalite to varying extent in both the massive and granular greenalite layers (see area 3, Fig. 2a). Both the coarse carbonate replacing greenalite and that in the fine-grained layers are sideritic (Fig. 3).

The second-lowest grade sample, B, is composed of granules that were probably originally greenalite but which have been replaced by sparry carbonate and chert. It also contains fragments of carbonate and fragments of chert partially replaced by carbonate (Fig. 2b). Hematite is present in both of these types of fragments; some is very fine-grained and probably primary, and some is coarser. Magnetite is widespread. By analogy with the Sokoman and Gunflint formations, the granules and fragments have been interpreted as current-deposited clasts of siliceous sediment derived from low- to high-energy sedimentary deposits within the Biwabik depositional basin (Lanier 1989; Simonson 1987). Some of the matrix is red-colored because of the presence of hematite, whereas elsewhere it is more chert-rich. Because of the occurrence of hematite and magnetite, oxygen fugacity was around that of the hematite-magnetite buffer (HM), the highest of any of our samples. Clasts contain carbonates of two or more compositions: (1) almost pure calcite (analysis 1, Table 1); and (2) two slightly different compositions of Fe-bearing dolomite (analyses 2 and 3, Table 1). Siderite is absent (Fig. 3). This is compatible with the observations of Floran and Papike (1978) in the Gunflint Iron Formation, who noted that at increasing metamorphic grade, siderite and ankerite disappear and calcite takes their place. The iron in this sample is present primarily in oxides and carbonates: the only Fe-bearing silicate is minor (1–2%) chlorite.

Sample C was collected from just above the hedenbergite-in isograd. It is composed of large crystals of hedenbergite growing over a matrix of quartz, magnetite, and minor actinolite (analysis 4, Table 1) and calcite (analysis 5, Table 1). The relict granular texture of the matrix is preserved by magnetite that outlines the granules and quartz that fills them (Fig. 2c). There is no measurable compositional zonation within the hedenbergite (analyses 6 and 7, Table 1).

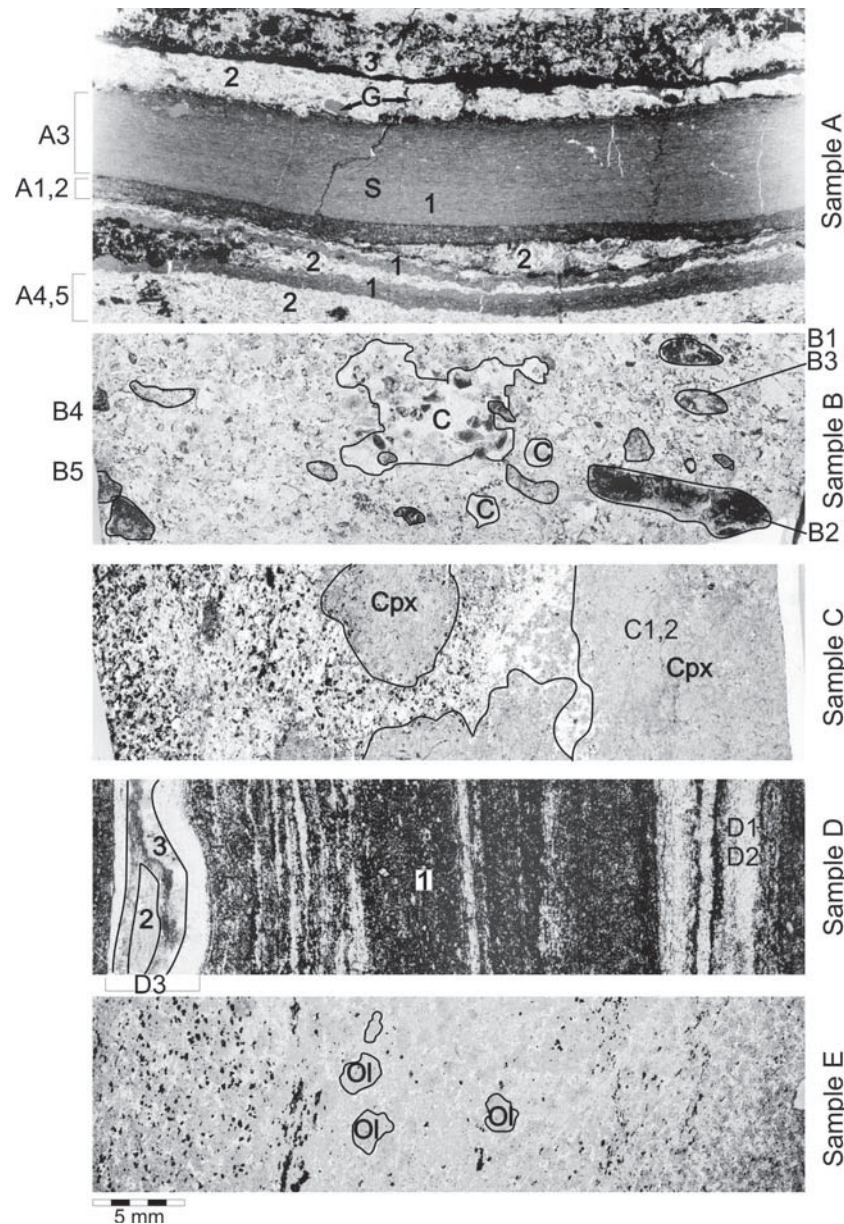


**Fig. 2** Transmitted light photomicrographs of samples analyzed in this study. Images are the length of a standard thin section (3.8 cm). Areas from which analyzed samples were taken are indicated with the sample number in *black*. **a** Lowest grade banded iron formation sample, composed of layers of sideritic carbonate (1) and greenalite (2). The thickest carbonate layer, marked “S”, contains no magnetite. Some greenalite granules are well-preserved (see examples marked “G”) but in some greenalite layers they are extensively replaced by magnetite (layer marked 3). **b** Oxidized, granular iron formation, composed of granules replaced with chert or carbonate and larger fragments (outlined by *thin lines*). Dark material in clasts and matrix is fine-grained hematite and magnetite. Several fragments

cemented with chert are indicated by “C”. **c** Hedenbergite-bearing granular iron formation, in which large hedenbergite crystals (marked “cpx”) overgrow a matrix dominated by quartz and magnetite with minor calcite and actinolite. **d** Grunerite-bearing banded iron formation, composed of thick layers of hedenbergite and magnetite (labeled 1) and thinner horizons composed of layers of grunerite (outer layers of sampled area D3), hedenbergite (labeled 3), carbonate and chert (labeled 2). **e** Fayalite-bearing iron formation composed of olivine (~40%), quartz (~45%) and magnetite (~15%) with minor grunerite and orthopyroxene. Some of the larger olivine grains are labeled. Magnetite is concentrated in bands in this rock

Sample D is a banded rock composed of two types of layers. Most of the rock is composed of thick horizons of magnetite interleaved with thinner layers of grune-

rite (analysis 8, Table 1) with minor apatite and actinolite (analysis 9, Table 1). Also preserved in this sample is a 2 mm-wide layer of chert and carbonate,

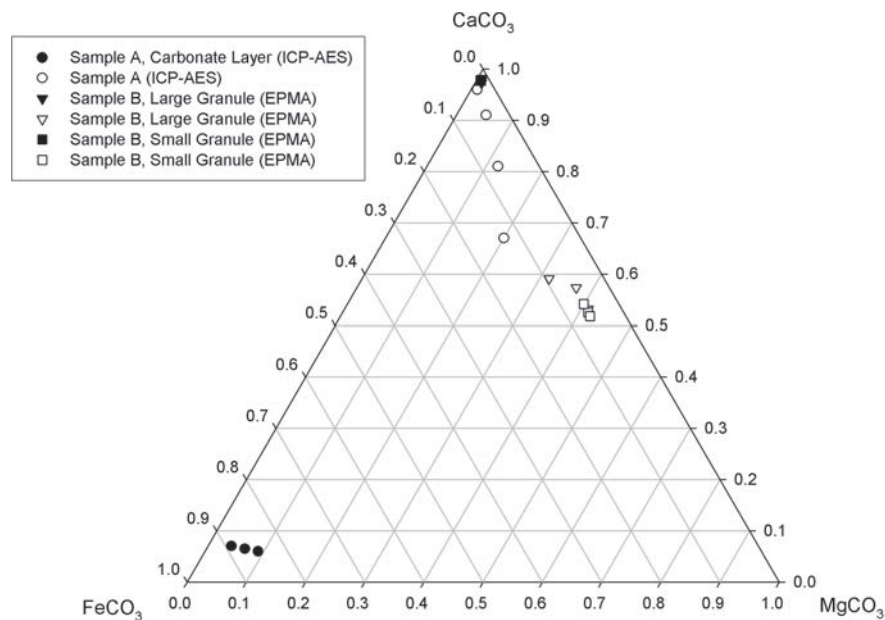


**Fig. 3** Carbonate compositions for several iron formation samples used in the Fe isotope study. Data for sample A was acquired by ICP-AES; samples B and C were acquired using the electron probe microanalyzer (EPMA). These data include measurements of MnO. This plot was constructed by normalizing  $\text{FeCO}_3 + \text{MgCO}_3 + \text{CaCO}_3 = 1.0$ . Sample B has coexisting

dolomite and calcite replacing greenalite granules. The carbonate analyses obtained by ICP-AES involved dissolution of carbonates and therefore the composition of the weighted average of the two carbonate minerals was obtained. Carbonates in sample A are siderite. Sample B carbonates are intermediate in composition between calcite and ankerite

rimmed by a 1 mm-wide layer of coarse-grained hedenbergite (analysis 10, Table 1), in turn rimmed by a 1 mm-wide layer of grunerite (Table 1; Fig. 2d).

Sample E is the highest-grade sample analyzed. It is composed of olivine, quartz and magnetite with minor grunerite (analysis 11, Table 1) and orthopyroxene (analysis 12, Table 1; Fig. 2e). In magnetite-rich layers, olivine is unzoned where it is adjacent to quartz (analyses 13 and 14, Table 1) but has a slightly more iron-rich rim where olivine is adjacent to grunerite (analysis 15, Table 1). This suggests that the zoning did not form during growth but instead reflects thermal diffusion at high temperature. Sample E has oxygen fugacity slightly above that of the fayalite-magnetite-quartz buffer (FMQ), which is the lowest of any sample analyzed here.

### Contact metamorphism of the Biwabik Iron Formation

The maximum temperatures attained across the contact aureole developed within the Biwabik Iron Formation can be estimated from phase relations within the systems  $\text{FeO-SiO}_2\text{-H}_2\text{O}$  and  $\text{CaO-FeO-MgO-SiO}_2$  (Fig. 4). Reaction curves for the system  $\text{FeO-SiO}_2\text{-H}_2\text{O}$  in Fig. 4 were calculated from the data of

Andersen et al. (1993), Berman (1988), Lattard and Evans (1992), and Rasmussen et al. (1998). The pressure of the contact aureole is constrained to lie between 1 and 3 kilobars, with 2 kilobar being perhaps the best estimate (Andrews and Ripley 1989). At these pressures, minnesotaite forms by reaction of greenalite with quartz [reaction i, Fig. 4] at around 160°C. Because Mg favors minnesotaite over greenalite, this is the high-temperature limit for the appearance of minnesotaite; it will form at lower  $T$  in more Mg-rich rocks. In the rocks from outside the contact aureole we have observed greenalite without minnesotaite, greenalite + minnesotaite, or minnesotaite without greenalite. This variation probably reflects differences in  $\text{FeO}/(\text{FeO} + \text{MgO})$  ratio of the rocks. O-isotope temperatures derived from data on magnetite-quartz pairs (Perry et al. 1973) and revised using the expression of Clayton and Keefer (1991) yield temperatures of around 200°C for the regional metamorphism. Natural greenalite contains significant amounts of ferric iron (Floran and Papike 1975) and this may explain the difference between the O-isotope temperature and theoretical breakdown curve for greenalite shown on Fig. 4.

The phase relations shown on Fig. 4 allow us to estimate the maximum temperature reached by each of

**Table 1** Representative mineral compositions, reported as oxide weight percents, anhydrous and without CO<sub>2</sub> included

	Sample B				Sample C				Sample D				Sample E			
	1	2	3	4	5	6	7	8	9	10	11	12	13	14	15	
SiO <sub>2</sub>	-	-	-	49.60	-	48.68	48.39	51.07	50.68	50.64	51.13	48.40	30.79	30.75	30.62	
Al <sub>2</sub> O <sub>3</sub>	-	-	-	0.23	-	0.02	0.03	0.28	1.58	0.13	0.41	0.13	-	-	-	
TiO <sub>2</sub>	-	-	-	0.03	-	0.02	0.02	0.00	0.00	0.00	0.00	0.00	-	-	-	
MgO	0.45	14.68	18.16	1.03	0.02	0.27	0.17	9.19	8.70	6.74	8.21	7.18	3.89	3.76	3.27	
FeO	1.32	6.93	4.68	33.30	0.53	27.78	28.35	35.72	25.15	20.28	36.69	42.36	64.41	64.68	65.17	
MnO	3.26	2.54	3.29	1.53	1.04	0.90	0.88	0.34	0.10	0.17	0.57	0.92	1.08	1.05	1.16	
CaO	59.02	36.75	31.99	11.43	62.56	22.22	22.06	0.94	10.34	21.55	0.91	1.09	0.04	0.05	0.04	
Na <sub>2</sub> O	-	-	-	0.10	-	0.11	0.11	0.15	0.71	0.40	0.18	-	-	-	-	
K <sub>2</sub> O	-	-	-	0.02	-	0.01	0.00	0.00	0.17	0.00	0.00	-	-	-	-	
Σ	64.05	60.90	58.12	97.27	64.15	100.01	100.01	97.69	97.43	99.91	98.09	100.08	100.21	100.29	100.26	

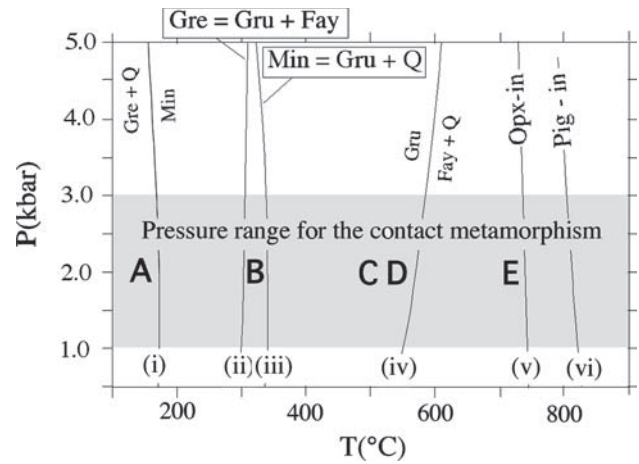


**Fig. 4** Phase relations for the system FeO–SiO<sub>2</sub>–H<sub>2</sub>O calculated from the data of Andersen et al. (1993), Berman (1988), Lattard and Evans (1992) and Rasmussen et al. (1998). The placement of letters A–E indicate the estimated peak metamorphic temperatures attained by these samples based upon their mineral assemblages

our analyzed samples. Sample A, which is located outside the contact aureole, and contains greenalite but no minnesotaite, could not have exceeded 200°C. We note, however, that in other rocks greenalite occurs in beds that lack quartz. In such an environment the upper thermal stability of greenalite may reach to temperatures above 300°C (reaction ii; Fig. 4).

Sample B comes from below the grunerite-in isograd. Reaction iii on Fig. 4 limits the conditions of the grunerite-in isograd to around 340°C. Two factors make this estimate uncertain. First, the presence of Mg in the system will stabilize minnesotaite to higher T. Second, much of the grunerite in the iron formation formed from siderite rather than minnesotaite. This means that there was CO<sub>2</sub> in the fluid, the presence of which would depress reaction iii to lower T. We therefore suggest a maximum temperature of 300 to 340°C for sample B during contact metamorphism.

The maximum temperature attained by sample C, which comes from just above the hedenbergite in isograd, is difficult to constrain. We have not shown a univariant reaction on Fig. 4 that can be used to estimate the temperature for the first appearance of hedenbergite because the hedenbergite-forming reaction must have involved carbonate, and therefore could not be plotted as a univariant curve in Fig. 4. The isograd occurs partway between the grunerite-in isograd [ca. 350°C and the fayalite in isograd (575°C) (Fig. 1)]. A reasonable, but highly uncertain, estimate for the temperature of this reaction is 500°C.

Sample D comes from just below the fayalite-in isograd and probably was metamorphosed to 500–550°C.

The first fayalite forms from breakdown of grunerite via reaction iv) on Fig. 4. This occurs at 550 to 580°C in the pure FeO–MgO–SiO<sub>2</sub>–H<sub>2</sub>O system. The presence of CO<sub>2</sub> in the fluid would cause this dehydration reaction to occur at lower *T*. However, this should not affect our temperature estimate because mineral assemblages in samples undergoing this reaction do not include carbonate, indicating that all the carbonate in the iron formation had been consumed by the time the fayalite isograd was reached. Thus, continued dehydration of the hydrous silicates should have driven the fluid to a water-rich composition by the time that olivine started to form. The temperature given by reaction iv) is a lower limit for fayalite because Mg strongly favors grunerite. Thus in more magnesian systems reaction iv) occurs at progressively higher *T*. In systems with sufficiently high Mg, breakdown of low-Ca amphibole forms orthopyroxene rather than olivine.

Based upon the coexisting olivine, orthopyroxene and grunerite (Table 1), we conclude that sample E attained temperatures of approximately 725–740°C (Evans and Ghiorso 1995), an estimate that is independent of pressure in the range of 2–5 kb.

## Analytical methods

### Sample preparation

Polished thin sections were made of each sample and the electron microprobe was used to estimate mineral abundances and compositions. A diamond wafer saw and tungsten carbide tipped micro-drill bit were used to separate mechanically layers of banded iron formation and to obtain separates rich in various silicates and oxides; these portions of the samples are indicated on Fig. 2. Magnetite was then removed from these samples magnetically and dissolved in 6M HCl. The remaining non-magnetic portion of the sample was subjected to a series of sequential dissolutions to isolate different mineral components. First, carbonate was removed from samples using 10% acetic acid. The sample in acetic acid was agitated ultrasonically for 1 h at room temperature, then left overnight. After centrifuging, the supernate solution was removed by pipette and the residue rinsed repeatedly with deionized water. Fe-oxides and greenalite were removed from samples by adding 1M HCl, and heating overnight at ~100°C. The supernate solution was removed by pipette after centrifuging and the 1M HCl treatment repeated. After the second addition of 1M HCl was removed, the residue was rinsed with deionized water. Any remaining sample was digested with HF. In sam-

ple E, quartz was removed from olivine and minor grunerite using heavy liquids. The olivine and grunerite fraction was then rinsed repeatedly with acetone prior to dissolution in HF–HNO<sub>3</sub>.

All dissolved mineral separates were analyzed for major element compositions by ICP-AES. We identified the composition of the carbonates from these analyses (Fig. 3). We also used these analyses to check the purity of the minerals that were dissolved in each step. The possible contamination of the acetic and hydrochloric acid leach steps with silicates was estimated from the Fe/Si ratios of these solutions. The amount of silicate Fe in the acetic and hydrochloric leach steps was calculated from the measured Si concentrations and the stoichiometric Fe/Si ratios of the silicate minerals. All acetic and hydrochloric leachates were estimated to contain less than 6% Fe from silicate minerals, except for HCl leachate D1.1 which was somewhat higher. These results give the maximum estimate of contamination because minor amounts of chert or quartz that is present in most of the layers was neglected for the calculations. Assessment of the presence of Fe-oxides in the acetic leachate (intended to separate carbonates) and the presence of undissolved carbonates in the hydrochloric leachate (intended to dissolve greenalite and Fe-oxides) is more difficult, but the major element compositions of the leachate solutions suggest that the stepwise leaching was successful. For example in sample B, acetic leachate solutions contained 220–970 ppm Ca with Fe/Ca ratios of 0.03–0.19 whereas the corresponding hydrochloric leachate solutions contained between 0.06 and 19 ppm Ca with Fe/Ca ratios of 75–3,640.

### Iron isotopic analysis

Fe was extracted from the samples using the procedures described in Schoenberg and von Blanckenburg (2005). The Fe separated from all samples was checked for purity by ICP-AES measurement prior to isotope analysis.

Fe isotope analyses were measured on a Thermo-Finnigan Neptune MC-ICP-MS in medium-resolution mode (Weyer and Schwieters 2003). All Fe isotopes were detected simultaneously in a first integration cycle together with <sup>52</sup>Cr and <sup>60</sup>Ni as monitors for the correction of isobaric interferences of <sup>54</sup>Cr on <sup>54</sup>Fe and <sup>58</sup>Ni on <sup>58</sup>Fe. In this study the instrumental mass bias was corrected using the Cu-doping technique (Arnold et al. 2004; Schoenberg and von Blanckenburg 2005) and thus <sup>65</sup>Cu and <sup>63</sup>Cu were measured during a second integration cycle. Merck CertiPUR Cu standard was added to all diluted Fe analytes (except for two samples

run at a later date) and to IRMM-14 and JM Fe standards to yield Fe and Cu concentration of 5 and 3 ppm, respectively. Fe isotope ratios of samples and standards were corrected for instrumental mass bias using a  $^{65}\text{Cu}/^{63}\text{Cu}$  ratio of 0.44513 and an exponential fractionation law. For the Cu doping method, Fe isotope data are expressed in the  $\delta$  notation as the ‰ deviation of the Fe isotope ratios of samples from the average of the respective ratios of their immediately preceding and following IRMM-14 standards, e.g., for  $\delta^{56}\text{Fe}$ :

$$\delta^{56}\text{Fe}_{\text{Sample}} = \left( \frac{{}^{56}\text{Fe}/{}^{54}\text{e}_{\text{Sample}}}{{}^{56}\text{Fe}/{}^{54}\text{Fe}_{\text{IRMM-014}}} - 1 \right) \times 1000 \text{ [‰]} \quad (1)$$

$\delta$ -values were calculated using both the Cu-corrected Fe isotope ratios of samples and bracketing IRMM-14 standards as well as their uncorrected raw Fe isotope ratios. The external reproducibilities for the Cu-corrected Fe isotope ratios are 0.042‰ for  $\delta^{56}\text{Fe}$  and 0.071‰ for  $\delta^{57}\text{Fe}$  and those for the raw Fe isotope ratios are 0.055‰ for  $\delta^{56}\text{Fe}$  and 0.092‰ for  $\delta^{57}\text{Fe}$  (2 standard deviations; Schoenberg and von Blanckenburg 2005). The reproducibilities of  $\delta$ -values calculated from raw Fe isotope ratios in this study by sample-standard bracketing are slightly inferior to those that can be achieved by standard-sample bracketing correction on Cu-free solutions. This is due to the increased analysis time of two cycle measurements when adding Cu (Schoenberg and von Blanckenburg 2005).  $\delta^{56}\text{Fe}$  and  $\delta^{57}\text{Fe}$  values obtained with both mass bias correction methods are in excellent agreement.

## Results

Iron isotope compositions of carbonate, silicate and oxide minerals separated from Biwabik Iron Formation samples vary from  $\delta^{56}\text{Fe} = -0.92$  to  $+0.82$ ‰ (Table 2). Bulk Fe isotopic compositions of each sample were estimated from the measured Fe isotopic composition of the constituent minerals and their modal abundance and Fe contents. In the case of layered samples A and D, bulk Fe isotopic compositions were estimated for each layer. These bulk Fe isotopic composition estimates listed on Table 2 are shown as bars on Fig. 5. It is immediately evident that the bulk compositions of the samples is not uniform, nor does bulk Fe isotopic composition correlate to metamorphic grade. Instead it is mainly a function of modal mineralogy: the carbonate-rich layers and samples have the lowest bulk  $\delta^{56}\text{Fe}$  values whereas magnetite-rich layers and samples have the highest bulk  $\delta^{56}\text{Fe}$  values.

The Fe isotopic compositions of minerals from Biwabik Formation yield some consistent features: magnetite is typically the isotopically heaviest mineral, while carbonate is almost always the lightest mineral. Silicates usually have intermediate compositions. The difference in  $\delta^{56}\text{Fe}$  between magnetite and silicates is as much as 0.8‰. Neither the absolute  $\delta^{56}\text{Fe}$  of a particular mineral nor inter-mineral differences correlates with metamorphic grade.

Several aspects of the iron isotopic data merit detailed description.

1. *Isotopic inter-layer heterogeneity* Substantial layer-to-layer heterogeneities are observed in the lowest grade, banded, iron formation sample (sample A). The bulk  $\delta^{56}\text{Fe}$  calculated from modal mineralogy varies from layer to layer (Fig. 5), and is higher in the silicate-rich layer than in the carbonate-rich ones. Three different layers were analyzed in this sample (Fig. 2). A sample of a thin carbonate-rich layer was cut from sample A. A1 is the non-magnetic portion of this layer.  $\delta^{56}\text{Fe}$  of carbonate dissolved from the non-magnetite separate is  $-0.64$ ‰. The residue remaining after dissolution of carbonate was dissolved in 1M HCl and appears to consist mainly of fine-grained greenalite and any residual magnetite that was not extracted magnetically. The  $\delta^{56}\text{Fe}$  of this material is  $\delta^{56}\text{Fe} = -0.32$ ‰. Fine-grained magnetite removed magnetically from this thin layer (A2.1) has a less negative  $\delta^{56}\text{Fe} = -0.14$ ‰. A3 is a sample of a thicker, oxide-free carbonate layer. Carbonate in this layer has  $\delta^{56}\text{Fe}$  of  $-0.74$ ‰, which is similar to the carbonate from the thin carbonate-rich layer (A1.1). Fine-grained greenalite has a negative  $\delta^{56}\text{Fe}$  of  $-0.78$ ‰. Minor chlorite in this thick carbonate layer has slightly higher  $\delta^{56}\text{Fe}$  of  $-0.37$ ‰. The estimate bulk  $\delta^{56}\text{Fe}$  of the silicate layer is much higher than those of the carbonate layers, and is due to abundant, isotopically heavy magnetite in this layer ( $\delta^{56}\text{Fe}$  of magnetite =  $+0.69$ ‰). Greenalite in the silicate layer has  $\delta^{56}\text{Fe} = -0.11$ ‰. We note that the magnetite in the silicate layer has an Fe isotopic composition that is much higher than magnetite in the thin carbonate layer ( $\delta^{56}\text{Fe} = -0.14$ ). Evidently, magnetite grains in adjacent layers are not in isotopic equilibrium. This suggests that the iron formation samples either (1) have protoliths with varying  $\delta^{56}\text{Fe}$ , such that carbonate-rich iron formation may have a bulk composition that is lighter than silicate-rich iron formation, or (2) that subsequent diagenetic and/or metamorphic processes have redistributed iron.

2. *Variations in Fe isotopic composition with increasing metamorphic grade* Contact metamorphosed iron formation samples show no simple relationship between metamorphic grade and Fe isotopic

**Table 2** Fe isotopic compositions of minerals composing Biwabik Iron Formation samples

Sample No.	Material	Fraction by wt	Treatment	Phase analyzed	SSB		Cu doping	
					$\delta^{56}\text{Fe}\text{‰}$	$\delta^{57}\text{Fe}\text{‰}$	$\delta^{56}\text{Fe}\text{‰}$	$\delta^{57}\text{Fe}\text{‰}$
<b>A: banded iron formation, peak <math>T &lt; 200^\circ\text{C}</math></b>								
Thin carbonate layer, estimated bulk $\delta^{56}\text{Fe} = -0.43\text{‰}$								
A1.1	Non-magnetic fraction	0.87	Acetic acid 1M HCl	Carbonate	-0.638	-0.925	-0.614	-0.889
A1.2	Non-magnetic fraction			Greenalite + minor magnetite	-0.315	-0.448	-0.326	-0.465
A2.1	Magnetic fraction	0.13	6M HCl	Magnetite	-0.144	-0.196	-0.153	-0.209
Thick carbonate layer, estimated bulk $\delta^{56}\text{Fe} = -0.76\text{‰}$								
A3.1	Thick carbonate		Acetic acid	Carbonate	-0.742	-1.105	-0.742	-1.105
A3.2	Thick carbonate		1M HCl	Greenalite	-0.788	-1.155	-0.786	-1.153
A3.4	Thick carbonate		HF	Chlorite	-0.372	-0.583	-0.379	-0.593
Silicate layer, estimated bulk $\delta^{56}\text{Fe} = +0.48\text{‰}$								
A4.1	Non-magnetic fraction	0.06	1M HCl	Greenalite	-0.112	-0.190	-0.118	-0.199
A5.1	Magnetic fraction	0.94	6M HCl	Magnetite	0.689	1.013	0.668	0.982
A5.4	Magnetic fraction		HF	Chert + residual magnetite	0.651	0.958	0.647	0.952
<b>B: oxidized, granular iron formation, peak <math>T &lt; 340^\circ\text{C}</math></b>								
Estimated bulk $\delta^{56}\text{Fe} = +0.13\text{‰}$								
*B1.2	0.2 cm-long hematite clast		1M HCl	Hematite	0.015	0.037	0.122	0.196
B2.1	0.5 cm-long clast		Acetic acid	Carbonate	-0.920	-1.336	-0.913	-1.326
B2.2	0.5 cm-long clast		1M HCl	Magnetite $\pm$ hematite	0.180	0.266	0.160	0.236
B2.4	0.5 cm-long clast		HF	Chlorite, chert	0.226	0.307	0.214	0.290
B3.1	0.3 cm-long clast		Acetic acid	Carbonate	-0.568	-0.871	-0.573	-0.877
B3.2	0.3 cm-long clast		1M HCl	Magnetite $\pm$ hematite	0.178	0.265	0.183	0.272
B3.4	0.3 cm-long clast		HF	Chlorite, chert	0.290	0.442	0.250	0.382
*B4.1	Red, granular matrix		Acetic acid	Carbonate	-0.586	-0.876	-0.430	-0.644
B4.2	Red, granular matrix		1M HCl	Magnetite $\pm$ hematite	0.174	0.269	0.187	0.290
B4.4	Red, granular matrix		HF	Chlorite, chert	0.265	0.355	0.261	0.349
B5.1	White, granular matrix		Acetic acid	Carbonate	-0.642	-0.953	-0.667	-0.989
B5.2	White, granular matrix		1M HCl	Magnetite $\pm$ hematite	0.119	0.159	0.120	0.160
B5.4	White, granular matrix		HF	Chlorite, chert	0.375	0.561	0.372	0.557
<b>C: hedenbergite-bearing granular iron formation, peak <math>T \sim 500^\circ\text{C}</math></b>								
Estimated bulk $\delta^{56}\text{Fe} = +0.33\text{‰}$								
C1.1	Non-magnetic fraction of hedenbergite-rich area	0.75	1M HCl	Calcite + magnetite	0.281	0.472	0.283	0.475
C1.4	Non-magnetic fraction of hedenbergite-rich area		HF	Hedenbergite	0.209	0.304	0.202	0.294
C2.1	Magnetic fraction of hedenbergite-rich area	0.25	6M HCl	Magnetite	0.444	0.672	0.441	0.667
C2.4	Magnetic fraction of hedenbergite-rich area		HF	Hedenbergite + residual magnetite	0.287	0.444	0.298	0.461

**Table 2** continued

Sample No.	Material	Fraction by wt	Treatment	Phase analyzed	SSB		Cu doping	
					$\delta^{56}\text{Fe}\text{‰}$	$\delta^{57}\text{Fe}\text{‰}$	$\delta^{56}\text{Fe}\text{‰}$	$\delta^{57}\text{Fe}\text{‰}$
<b>D: grunerite-bearing banded iron formation, peak <math>T &lt; 550^\circ\text{C}</math></b>								
Silicate layer, estimated bulk $\delta^{56}\text{Fe} = +0.76\text{‰}$								
D1.1	Non-magnetic fraction	0.07	1M HCL HF	Magnetite, minor apatite Grunerite + minor actinolite	0.697 0.566	1.076 0.857	0.705 0.560	1.089 0.848
D2.1	Magnetic fraction	0.93	6M HCL HF	Magnetite Grunerite + minor actinolite + residual magnetite	0.820 0.607	1.297 0.847	0.857 0.615	1.352 0.859
Carbonate layer, estimated bulk $\delta^{56}\text{Fe} = +0.69\text{‰}$								
D3.1	Carbonate-quartz-grunerite-hedenbergite layer		Acetic acid	Carbonate	-0.002		-0.010	
D3.2	Carbonate-quartz-grunerite-hedenbergite layer		Bulk dissolution	Bulk sample	0.688		1.017	
<b>E: olivine-bearing iron formation, peak <math>T &lt; 740^\circ\text{C}</math></b>								
Estimated bulk $\delta^{56}\text{Fe} = -0.06\text{‰}$								
E1.1	Magnetic fraction	0.14	6M HCL HF	Magnetite Silicates + residual magnetite	0.191 0.013	0.265 0.064	0.212 -0.013	0.296 0.026
E2.4	Olivine + grunerite separate	0.86	HF	Olivine + minor grunerite	-0.184	-0.196	-0.194	-0.211

Uncertainties on isotopic measurements are less than the external reproducibilities for Cu-corrected Fe isotope ratios of 0.042‰ for  $\delta^{56}\text{Fe}$  and 0.071‰ for  $\delta^{57}\text{Fe}$

\*Two samples, B1.2 and B4.1, contained very little iron and concentration matching between samples and IRMM-014 within 10% that is required for highly accurate measurements could not be achieved. Cu-doping correction for instrumental mass bias was preferred for these samples, whereas SBB is used in the discussion and figures of all other samples

characteristics (Fig. 5; Table 2). In the lowest-grade contact-metamorphosed sample, B, the  $\delta^{56}\text{Fe}$  of a clast composed of hematite is indistinguishable from  $\delta^{56}\text{Fe}$  in clasts rich in magnetite, or from the  $\delta^{56}\text{Fe}$  of magnetite in the granular matrix of this sample:  $\delta^{56}\text{Fe}$  of magnetite varies from  $\delta^{56}\text{Fe}$  of 0.12 to 0.19‰, and  $\delta^{56}\text{Fe}$  of hematite = 0.12‰. These values are intermediate between those from sample A, where  $\delta^{56}\text{Fe}$  of magnetite in the silicate layer is considerably heavier and that in the thin carbonate layer is lighter. On the other hand, although the carbonate in sample B is Fe-poor, the  $\delta^{56}\text{Fe}$  of its carbonates are comparable to those of the siderites from sample A (Fig. 5). Interestingly, in sample B  $\delta^{56}\text{Fe}$  of the silicate mineral, chlorite, is higher than  $\delta^{56}\text{Fe}$  of its oxide minerals, magnetite and hematite. This is the reverse of what is observed in all other samples, in which  $\delta^{56}\text{Fe}$  of silicate is lower than  $\delta^{56}\text{Fe}$  of magnetite. The bulk  $\delta^{56}\text{Fe}$  calculated for this sample of +0.1‰, which is intermediate between the calculated bulk  $\delta^{56}\text{Fe}$  of the carbonate layers and the silicate layer in sample A.

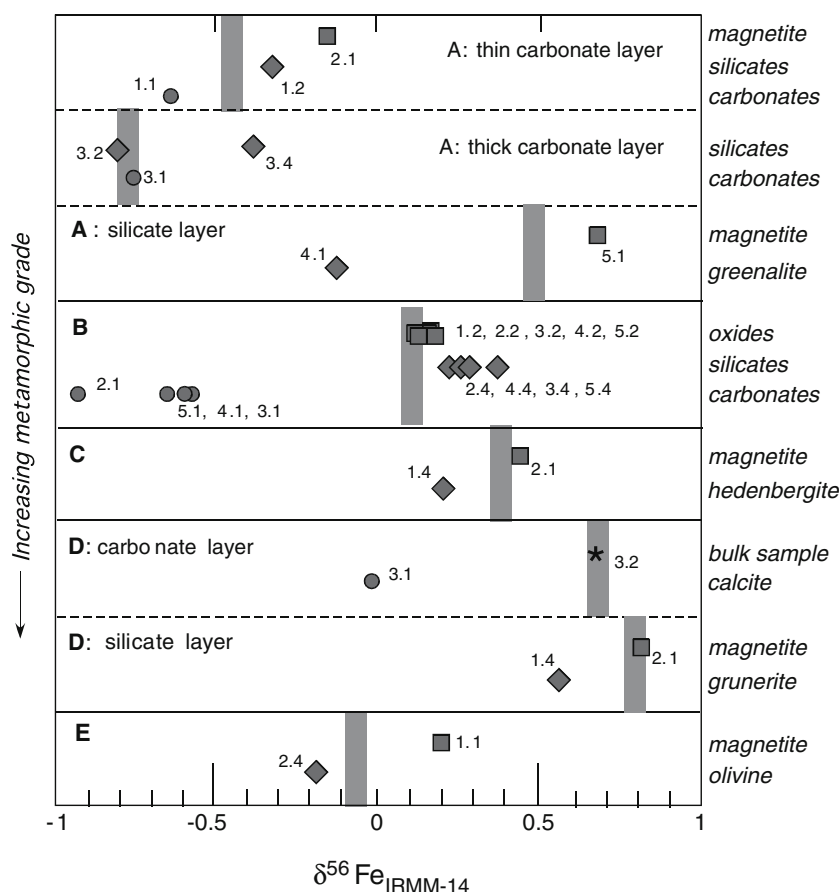
In the higher-grade contact-metamorphosed samples, the  $\delta^{56}\text{Fe}$  of the magnetite varies significantly but does not correlate with estimated metamorphic temperature.  $\delta^{56}\text{Fe}$  of magnetite is lightest (+0.19‰) in the

highest-grade sample E, heaviest (+0.82‰) in the second-highest grade sample D, and intermediate (+0.44‰) in sample C. The  $\delta^{56}\text{Fe}$  of the metamorphic Fe-silicates are  $\delta^{56}\text{Fe} = -0.18$ ‰ for olivine, +0.57‰ for grunerite, and +0.21‰ for hedenbergite. Carbonate has been completely consumed in these samples except in a 0.3 cm thick horizon in sample D. The calcite in this horizon has  $\delta^{56}\text{Fe} = 0.00$ ‰. The calculated bulk  $\delta^{56}\text{Fe}$  of these samples varies from approximately  $\delta^{56}\text{Fe} = 0.75$ ‰ for D to  $\delta^{56}\text{Fe} = 0.33$ ‰ for C to  $\delta^{56}\text{Fe} = -0.06$ ‰ for E.

### Discussion

The results presented above illustrate that although iron formation is chemically simple, these rocks are clearly complex in terms of the processes that involve iron and potentially fractionate iron isotopes. We may identify three periods during which iron may be redistributed in Biwabik Iron Formation: (1) during primary deposition of the iron formation and early diagenesis, (2) during later diagenesis, perhaps up to and including low-grade regional burial metamorphism, and (3) during contact metamorphism.

**Fig. 5** Fe isotope variations in minerals from samples of Biwabik Iron Formation. Estimated bulk compositions for each sample or layer are shown as vertical bars. Squares denote data from oxides, diamonds represent silicates, circles represent carbonates, and star represents a bulk rock measurement. The uncertainties are approximately the size of the symbols. The numbers next to each symbol are the analysis number listed on Table 2



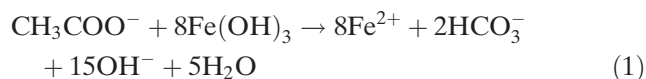
## Deposition and early diagenesis of banded iron formation

It has been suggested that BIF precipitated from seawater rich in dissolved, hydrothermally sourced ferrous Fe and close to silica-saturation. Dissolved silica, when at saturation, would react with iron to form amorphous iron-silicate gels (Konhauser et al. 2002). These would readily react to form early diagenetic minerals, including chert, greenalite, siderite and hematite (Klein 2005). The sedimentology of iron formation indicates that these reactions probably occurred in a variety of subtidal environments (Simonson 1985). Finely banded iron formation consisting of chemical mud may have been deposited in quiescent environments well below wave-base. On the other hand, iron formation that is composed of rip-up clasts and well-sorted greenalite granules may have formed originally on shallow, high-energy shelves. These chemical sediments were probably originally deposited in relative quiet water, and were reworked by turbulent currents. These greenalite granules were then washed down and deposited on top of lutitic horizons, probably during storm events. The fact that the granules are typically uncompacted suggests that these layers underwent early silica cementation (Lanier 1989).

The primary Fe-silicate mineral in Biwabik Iron Formation is greenalite, which is typically fine-grained, and brownish green. As noted above, most of the greenalite in the Biwabik Iron Formation is detrital in origin, occurring as sand-sized granules. We have recognized one occurrence of massive greenalite, but textures indicate that this could have formed from compacted granules. We conclude that greenalite was initially precipitated elsewhere, lithified, rolled and sorted, and then re-deposited as sand-sized granules (Gundersen and Schwartz 1962). These greenalite sands were then cemented by chert to form layers that typically are 5 mm to 5 cm thick (Gundersen and Schwartz 1962; this study). Sparse greenalite granules are present in some carbonate layers, but these are relatively rare.

Sideritic carbonate is a major phase within the finely-laminated lutitic layers. It typically forms thin, millimeter- to centimeter-thick layers between the thicker layers of greenalite granules. The siderite is typically micritic, but locally it is pelloidal, pisolitic, and rarely oolitic. It is present in sample A, together with fine-grained iron-bearing minerals and chert. The thin carbonate layer in sample A contains magnetite, but the thick carbonate layer immediately adjacent does not. This observation is in accordance with those of James et al. (1968), who observed that whereas the mineral constituents of a given layer tend to be uni-

form laterally, they can change abruptly from layer to layer. Although it has been proposed that siderite precipitates as primary phase from seawater (Klein 2005), some siderite could represent an early diagenetic phase resulting from microbial oxidation of organic matter and the simultaneous reduction of Fe(III) hydroxides (Lovley 1990). The latter hypothesis is supported by the fact that in samples of low-grade Biwabik Iron Formation, most siderite layers contain dark brown kerogen on carbonate grain boundaries. This hints at the possible involvement of microbes during diagenesis. Siderite formation during oxidation of organic matter by dissimilatory iron reducing microbes (DIR) is possible at elevated pH according to the following reaction hydroxides (Lovley 1990):

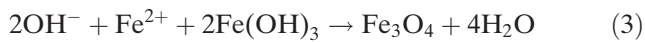


This microbially mediated reaction results in the presence of a high pH at the surface of Fe(III) hydroxide. The high pH and the high bicarbonate content facilitates the precipitation of siderite:



One of the earliest diagenetic minerals is fine-grained quartz, which in many layers was deposited in the interstices of the greenalite sand before the granules had undergone compaction. Another early diagenetic mineral, hematite, is present as clasts and as fine, dusty material within clasts in relatively oxidized iron formation (sample B). Most probably hematite is an early diagenetic product of the crystallization of amorphous Fe(III) oxy-hydroxides.

French (1968) concluded that very fine-grained magnetite crystals (5 microns or less in size) in the Biwabik Formation could be primary but that the far more common, coarser euhedra, 0.05–0.1 mm in size, were secondary. Klein (2005) has speculated that magnetite might form from a primary hydromagnetite precursor. More likely is an early diagenetic origin. Microbiological studies suggested that primary magnetite of nanometer size might precipitate intracellularly by magnetotactic bacteria (Konhauser 1998). However, a 5,000 times higher production rate of secondary diagenetic magnetite, also of nanometer size, was suggested to take place by extracellular processes by dissimilatory iron reduction (Lovley et al. 1987). The required conditions are the close association of Fe(II) and Fe(III) at high pH, which is the result of the activity of Fe(III)-reducing microorganisms. The magnetite-forming reaction is



Magnetite can compete with siderite for Fe(II) (Lovley 1990), and often both occur in association. This is essentially the Fe(III)-reducing process that was calibrated for Fe isotopes (Johnson et al. 2005b). Evidence for this reaction is found in the association of magnetite with carbonates low in  $\delta^{13}\text{C}$  (Lovley 1990).

Identification of the Fe isotopic fractionations associated with the primary deposition and early diagenesis of iron formations is problematic. As we discuss below, iron has undergone extensive mobilization during later diagenesis and regional burial metamorphism of the Biwabik Iron Formation, making it difficult to see through these effects in order to identify the primary and early diagenetic isotopic composition of the iron.

Of our suite, only samples A and B might preserve iron isotopic compositions of primary and early diagenetic minerals. As described above, sample A contains alternating micritic carbonate layers and layers of greenalite sand, whereas B is a hematite-bearing, carbonate-rich breccia. There is no question that the layering in sample A and the clasts and fragments in sample B are primary depositional features. Therefore, the observed variations in  $\delta^{56}\text{Fe}$  could reflect primary isotopic heterogeneity in the composition of magnetite, siderite and greenalite deposited in different layers and fragments. However, because the rocks have been subject to later diagenetic and low-grade regional metamorphism, it is possible that there has been some later redistribution of iron isotopes that has affected their isotopic composition.

If the  $\delta^{56}\text{Fe}$  of greenalite, siderite, hematite and magnetite are the result of primary to early diagenetic processes, then we must explain the major variations in  $\delta^{56}\text{Fe}$  between samples, and between layers and clasts within low-grade samples A and B. For example, in sample A, the  $\delta^{56}\text{Fe}$  of magnetite in a greenalite layer is 0.83‰ higher than magnetite in a carbonate-rich layer. This difference in the iron isotopic composition of magnetite from immediately adjacent layers represents a third or more of the total variation observed in magnetite from other iron formations worldwide. Rouxel et al. (2005) documented variations in  $\delta^{56}\text{Fe}$  of magnetite from four different Late Archean and Early Proterozoic BIF of slightly less than 2.5‰. Johnson et al. (2003) observed variations of as much as 1.7‰ in the  $\delta^{56}\text{Fe}$  of magnetite from the Groenwater member of Transvaal Supergroup BIF in samples separated stratigraphically by only 34 m.

If these variations reflect original, primary heterogeneities, then there are two possible explanations. The first is that the layer-to-layer heterogeneities re-

fect differences in the Fe composition of the source from which they were delivered or the fluid from which they were precipitated. In the Biwabik Iron Formation, it is likely that the carbonate-rich layers were originally deposited in quiet, presumably deeper waters than greenalite. It is possible that the shallow waters from which the greenalite precipitated had a different composition than the waters from which the carbonate precipitated, producing different bulk  $\delta^{56}\text{Fe}$  for each layer. For example the carbonate Fe may be dominated by hydrothermal Fe, which has today a  $\delta^{56}\text{Fe}$  composition of roughly  $-0.5\text{‰}$  (Sharma et al. 2001), while greenalite might comprise a mixture of terrigenous and hydrothermal sources. It is possible that the iron isotopic composition of seawater would be affected by fractionation processes taking place within the water column. Oxidation of  $\text{Fe}(\text{II})_{\text{aq}}$  would produce  $\text{Fe}(\text{III})_{\text{aq}}$  that is 2.9‰ heavier (Welch et al. 2003; Anbar et al. 2005). Precipitation of such insoluble  $\text{Fe}(\text{III})_{\text{aq}}$  into ferrous (hydr)oxides would produce a precipitate that is up to 1.5‰ lighter than  $\text{Fe}(\text{III})_{\text{aq}}$  (Bullen et al. 2001; Skulan et al. 2002). Assuming that the reaction does not go to completion, then a ferrous precipitate would leave a light seawater residue behind. Rouxel et al. (2005) suggested that a Rayleigh distillation process driven by Fe oxide deposition could decrease the  $\delta^{56}\text{Fe}$  of seawater, which in turn would lead to subsequent precipitation of isotopically light oxide and sulfide minerals. They suggested that the competitive effects of episodic Fe supply from hydrothermal sources and Fe oxide precipitation would cause both Fe concentration and Fe isotopic composition of Precambrian seawater to fluctuate. These processes might potentially act on short time scales if the ocean is partially oxidised (Johnson et al. 2003) and could therefore change the Fe content and Fe isotopic composition of the oceans, producing the observed stratigraphic variations in  $\delta^{56}\text{Fe}$  of Fe-minerals in BIF and other seafloor sediments. It is tempting to invoke a light seawater residue to explain some of the light layer compositions, whereas the heavy layers could have been precipitated from oxidized seawater.

Alternatively, the Fe isotopic composition of seawater may have been uniform, and the observed variations in  $\delta^{56}\text{Fe}$  are simply a function of the different fractionation factors of the different mineralogies that compose the individual layers. For example, the primary carbonates in sample A are isotopically light simply because the equilibrium fractionation factors for these minerals are different than for other minerals such as magnetite. Siderite precipitated from  $\text{Fe}(\text{II})_{\text{aq}}$  is predicted from spectroscopic data to be approximately 1.5‰ lighter in  $\delta^{56}\text{Fe}$  than the iron dissolved in

the fluid (Polyakov and Mineev 2000; Schauble et al. 2001). A preliminary experimental determination of this isotope fractionation resulted in  $\Delta_{\text{siderite-Fe(II)aq}}$  of  $-0.5\text{‰}$  (Wiesli et al. 2004). Similarly, the Fe oxides measured in our samples are all heavier than both carbonate and greenalite because oxide precipitation favors heavy Fe (e.g., Polyakov and Mineev 2000). In this model, the isotope composition of each layer is controlled by its mineralogy and the relative modes of the minerals occurring in it.

A variant of this model is a scenario in which isotope fractionation occurs during early diagenesis. This model was explored in detail by Johnson et al. (2005b). Fe(III) hydroxide reduction by dissimilatory iron reduction (Lovley 1990; Lovley et al. 1987) would result in the formation of Fe(II)<sub>aq</sub> that is 2–3‰ lighter in  $\delta^{56}\text{Fe}$  than the Fe(III) substrate. Carbonate that precipitated from this fluid is between 0 and 1‰ lighter than the fluid, while magnetite would be 1.3‰ heavier (Johnson et al. 2005b). Overall, Fe incorporated into all these minerals would be lighter than the original oxide substrate, but carbonates would always be lighter than magnetite. This pattern is observed in the Biwabik samples, as well as in BIF minerals of Kapvaal samples (Johnson et al. 2003). Magnetites that have formed without this reductive process involved would incorporate heavier iron (Johnson et al. 2005b). The iron isotope composition of silicate minerals that would be predicted by this model is less clear. No data on the fractionation of greenalite from fluid exists, but in general silicates containing Fe(II) are predicted to obtain light Fe in equilibrium as compared to Fe(III) fluids and minerals (Polyakov and Mineev 2000). Their composition should be similar to that of carbonates, and this is in general agreement with our analyses. We expect some form of isotopic equilibrium involving greenalite, despite its presumably detrital origin, because as will be shown below, greenalite participates in diagenetic reactions breaking down to siderite or magnetite.

The discussion above suggests that it is possible to interpret the observed variations in  $\delta^{56}\text{Fe}$  as primary isotopic heterogeneities. However, because the rock has been subject to significant later diagenetic and low-grade regional metamorphism, we must examine the possibility that redistribution of iron during these subsequent events has totally overprinted their original isotopic compositions.

#### Diagenetic processes

It is clear from textural evidence that most of the magnetite in the Biwabik Iron Formation formed during late diagenesis or regional, low-temperature burial meta-

morphism. Previous workers on the Biwabik have presented three arguments for the late diagenetic origin of coarse-grained magnetite. First, coarse magnetite euhedra overgrow and pseudomorph primary greenalite (LeBerge 1964; French 1968; Floran and Papike 1975) and these magnetites are texturally similar to those growing along the margins of siderite horizons. Second, and most important, the coarse magnetite euhedra in the Biwabik have overgrown finer grains of hematite (Han 1978). Finally, there are a few localities in the unmetamorphosed Biwabik Formation that are unusually poor in magnetite. Magnetite in these rocks forms thin overgrowths on the primary greenalite and siderite minerals, suggesting that the primary sedimentary assemblage contained little magnetite (Juneau 1979).

In our samples we have observed that greenalite has been partially or totally replaced by coarse, sparry carbonate (both siderite and ankerite), coarse, euhedral magnetite, and quartz (Fig. 6a–d). Carbonate layers are variably replaced by magnetite. Some layers show large subhedral magnetite crystals replacing fine-grained carbonate (Fig. 6e), and other carbonate layers are cross-cut by magnetite veins (Fig. 6f). These textures and inferred diagenetic reactions in the iron formation discussed below amply demonstrate that diagenesis was associated with extensive element mobility. Importantly, the progress of these diagenetic reactions was variable, both in terms of degree of completion and length-scale. For example, in sample 97LTV9 (Fig. 6g) a 5 mm-thick layer of greenalite granules with thin rims of magnetite (center-right of figure) is immediately adjacent to a layer in which greenalite is almost entirely replaced by magnetite (center left, Fig. 6g). In addition, hematite persists in an adjacent silicified layer (right, Fig. 6g), suggesting that no diagenetic fluids penetrated this part of the rock. All of these features indicate that the mobility of iron and the oxidation state of the fluids during late diagenesis varied on the scale of mm. Therefore, these diagenetic reactions must have taken place after at least some of the layers were effectively sealed, such that diagenetic fluids could move only through the remaining, variably permeable layers. We suggest that primary sedimentary heterogeneity is one important factor controlling the progress of diagenetic reactions in each layer, which in turn is a function of differences in abundance of carbonate, greenalite, hematite, and organic material.

We recognize three major reactions that occurred during late diagenesis: (1) replacement of greenalite by silica, (2) replacement of greenalite by carbonate, and (3) formation of magnetite.

1. *Formation of silica* In addition to deposition of chert in the interstices of the greenalite sands, which

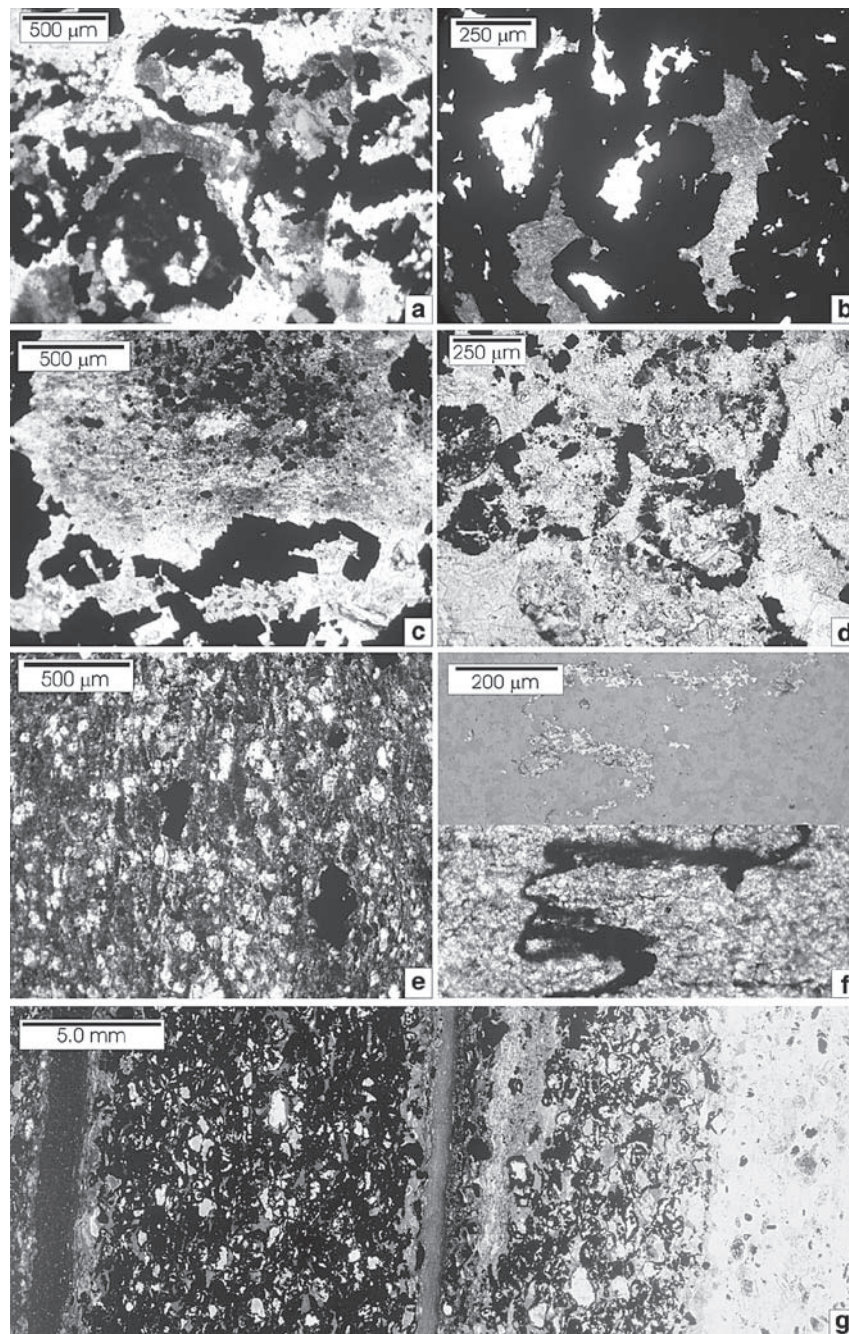
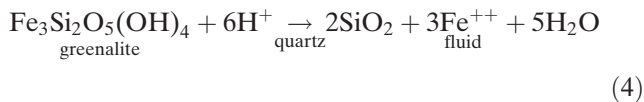


**Fig. 6** Transmitted light photomicrographs showing textural relations in low-temperature iron formation samples from outside the contact aureole. **a** Greenalite granules replaced with magnetite rims and cherty fillings. The largest granule near the bottom of the image contains remnant greenalite. One granule is partially filled with carbonate crystals. Sample (96B12C) was collected from the National Steel Pellet Mine, Kewatin MN, 65 km west of the edge of the contact aureole. **b** Magnetite replacing greenalite granules. The *gray filling* is greenalite, the *transparent filling* is quartz. Sample 97LTV34, location shown on Fig. 1. **c** A large granule replaced by quartz, magnetite, minor carbonate and very small, dusty grains of hematite. Sample 97LTV10, location shown on Fig. 1. **d** Granules almost completely replaced by carbonate and minor quartz, and rimmed by euhedral grains of magnetite.

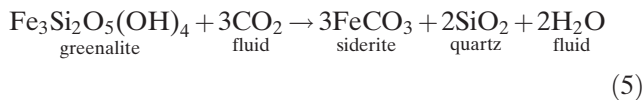
Sample B. **e** Large blocky opaque grains of subhedral magnetite replacing fine-grained siderite. Minor amounts of fine-grained iron silicate minerals are also present in the matrix. Sample 96LTV13, location shown on Fig. 1. **f** Portion of a small magnetite vein that cross-cuts the large siderite layer in sample A (see center-right of full-section image, Fig. 2a). The top portion of this image is reflected light, and the lower portion is the same view in transmitted light. **g** Full-section image of sample 97LTV9 (location on Fig. 1), showing variable progress of diagenetic reactions. Hematite is preserved in the 5 mm-wide silicified layer at the right end of the image, and greenalite granules have only thin magnetite rims in the 5 mm-wide layer adjacent. However, the greenalite granules on the left of the image are almost completely replaced with magnetite

we interpret as an early diagenetic feature, it is common to see greenalite being replaced by silica (Fig. 6a, b). The simplest reaction to write for this incongruent dissolution of greenalite is:



We balance this reaction using  $\text{Fe}^{++}$  as the mobile ion even though it is likely that iron was speciated with chlorine or an organic complex. At any rate, regardless of the speciation, it is clear from the textures that iron has been mobile. Reaction 4 involves a 78% decrease in the volume of solids. Because the chert pseudomorphs after greenalite granules have the same nearly circular cross-section as the primary granules, it is clear that reaction 4 isn't the only reaction taking place in the dissolution of greenalite. Silica in addition to that which was originally tied up in greenalite has to be added to the granule pseudomorphs.

2. *Formation of siderite* The alteration of greenalite to siderite can be modeled by the following reaction:



If the stoichiometry of the greenalite breakdown occurred exactly as written in equilibrium (5), then greenalite granules would be replaced by siderite-quartz intergrowths that consist of 66% siderite and 34% quartz. It is rare to find such relations; in most pseudomorphs the greenalite has been totally replaced either by quartz (Fig. 6a, b) or by siderite (Fig. 6d). This means that in the latter case, the alteration of greenalite to siderite commonly involves removal of silica.

3. *Formation of magnetite* We recognize three processes by which magnetite may have formed in the iron formation: (a) it could have been reduced from hematite, (b) it could have grown by oxidation of ferrous iron in siderite and greenalite or (c) it could have grown by oxygen-conserving reactions involving hematite with siderite or greenalite.

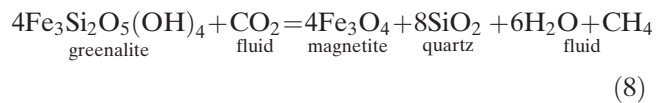
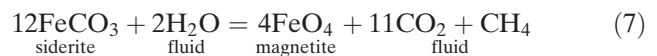
(a) *Reduction of hematite* One possible means of the formation of magnetite would be reaction between hematite and organic matter in the rocks. This reaction can be written as



It is possible that some magnetite in sample B formed by this reaction, because in this rock some of the

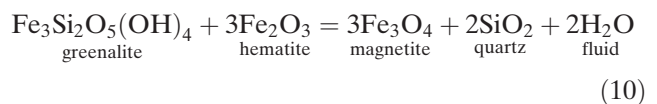
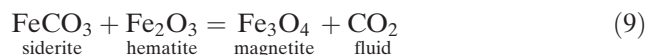
magnetite is fine-grained and intimately associated with hematite (Fig. 2). However, we conclude that the majority of the magnetite in the Biwabik Formation did not form in this way because of textural evidence showing magnetite growth on siderite and greenalite.

(b) *Oxidation of ferrous iron* As noted above, the dominant textures in the iron formation indicate that magnetite replaced greenalite or siderite. In discussing these reactions we must keep in mind that the reactions must involve an oxygen donor because oxygen abundance in the fluid is vanishing small (Frost 1992a). The most likely donor in iron formations involves the formation of methane from water and carbon dioxide. Two possible reactions are:



The best textural evidence for the presence of these reactions (especially reaction 8) is the presence of magnetite veins (Fig. 6f). These reactions may also have been the source of silica and carbon dioxide required for reactions 4 and 5. These reactions may have been biotically mediated, a likely occurrence considering the abundance of kerogen in many of the samples and the common occurrence of microfossils within the Biwabik and Gunflint Iron Formations (Lanier 1989; Chang et al. 1989). However, considering that the carbon isotopic compositions of carbonate from the Biwabik, correlative Gunflint, and other iron formations are heavier ( $\delta^{13}\text{C} = -8$  to  $-1\%$ ) than those that would have been deposited in association with biogenic methane (Perry et al. 1973; Winter and Knauth 1992; Klein 2005), these methane-forming reactions were either minor or occurred on a scale smaller than that indicated by earlier isotopic studies.

(c) *Reactions of hematite with siderite and greenalite* Another way to produce magnetite is through reactions between hematite and a source of ferrous iron. Two of the most likely are



Reactions 9 and 10 explain the textures observed in most samples described in this study and the textures indicating that magnetite in unmetamorphosed iron formations nucleated on hematite (Han 1978). Because all the ferric iron for the formation in these reactions is donated from hematite, these reactions are accompanied by a 47% volume increase in the abundance of iron oxides.

Unlike reactions 7 and 8 which may be bacterially mediated, reactions 9 and 10 are likely to occur in response to regional, burial metamorphism as the siderite–hematite and greenalite–hematite–quartz buffering surfaces crossed the hematite–magnetite buffer (Frost 1979). As noted above, magnetite–quartz oxygen isotope thermometry (Perry et al. 1973) indicates that the regional metamorphic temperatures were around 200°C.

Because of the high degree of elemental mobility that accompanied diagenesis of the Biwabik Iron Formation, it is very likely that the movement of iron during diagenesis and growth of magnetite controlled the observed  $\delta^{56}\text{Fe}$  and modified any primary and early diagenetic variations in iron isotope compositions. We also observe tremendous layer-to-layer heterogeneities in oxygen fugacity. For example, samples from the amphibole and hedenbergite zones possess millimeter- to centimeter-scale variation in the  $X_{\text{Fe}}$  of the silicates, hence a corresponding variation in  $f(\text{O}_2)$ . For example, one sample preserves a gradient over 5 mm of thin section from a layer containing clinopyroxene and actinolite ( $X_{\text{Fe}}$  in both minerals ~0.4) together with abundant magnetite, to a layer with hedenbergite and ferroactinolite ( $X_{\text{Fe}} = 0.97$ ) with no magnetite. We attribute these differences to differences in the progress of the original magnetite-forming reactions from layer to layer. These relations indicate minimal equilibration of Fe and  $f(\text{O}_2)$  across the layers. The variations in diagenetic reaction progress suggest that fluid flow was layer-parallel and that there was not likely much transport of Fe and Si perpendicular to the layering. The implication, therefore, is that the isotopic composition of iron also may be locally controlled by reactions within the layers. This is a likely explanation for the 0.83‰ difference in the  $\delta^{56}\text{Fe}$  of magnetite from adjacent layers in sample A. It also suggests that  $\delta^{56}\text{Fe}$  of magnetite may be quite different from place to place, and that these heterogeneities predate any subsequent redistributions during contact metamorphism.

The observed  $\delta^{56}\text{Fe}$  values of minerals in low-grade samples A and B are in general agreement with the hypothesis that these  $\delta^{56}\text{Fe}$  are the result of

iron isotopic equilibration during diagenesis. For example, in the greenalite layer of sample A, magnetite has higher  $\delta^{56}\text{Fe}$  than greenalite. In the thin carbonate layer, the relative order of  $\delta^{56}\text{Fe}$  is magnetite > Fe-silicate  $\geq$  carbonate. This relative order is consistent with the observations of Johnson et al. (2003) and with the theoretical predictions from spectroscopic data (e.g., Polyakov and Mineev 2000; see Polyakov et al. 2005 for a downward revision of the magnetite  $\beta$ -factor), and suggests that the isotopic difference between minerals may be controlled by equilibrium fractionation. In sample B, chlorite has higher  $\delta^{56}\text{Fe}$  than magnetite, and both are heavier than carbonates. The isotopically heavy chlorite is possibly consistent with the presence of ferric iron, which is correlated with isotopically heavier  $\delta^{56}\text{Fe}$  (see discussion in Schauble 2004, also Polyakov and Mineev (2000) predict compositions that are heavier than the revised magnetite value for ferric silicate minerals). Magnetite and hematite have similar  $\delta^{56}\text{Fe}$ , which agrees with revised fractionation factors for magnetite (Polyakov et al. 2005). Overall, there is general agreement between the observed mineral  $\delta^{56}\text{Fe}$  and empirical and theoretical equilibrium fractionation factors in both samples A and B.

It cannot be overemphasized that although within layers the minerals may have attained isotopic equilibrium during diagenetic reactions, no such equilibrium was achieved from layer-to-layer or sample to sample. We have observed that the bulk  $\delta^{56}\text{Fe}$  is different for the three different layers analyzed in sample A, and for sample B. These heterogeneities indicate that the isotopic composition of iron is controlled by diagenetic fluids and reactions, and that these vary from layer-to-layer. Evidence from low-temperature samples A and B indicates that these heterogeneities were established during deposition and diagenesis, prior to contact metamorphism.

## Metamorphic processes

### *General principles*

There are several possible mechanisms that control the stable isotopic composition of metamorphic minerals. Gilletti (1986) recognized that coexisting minerals will not establish isotopic compositions that correspond to equilibrium fractionation factors unless all minerals are open to element exchange. We can envision four possible models for Fe isotope exchange between metamorphic minerals, depending upon whether they are open to Fe diffusion or not during dissolution–precipitation processes (Fig. 7).



thermometry, Fe–Ti oxides will be open to diffusion to lower temperatures than silicates (e.g., Frost et al. 1988).

Several workers have noted that available diffusivity measurements (Freer and Hauptman 1978) vastly overestimate the diffusivity of magnetite due to the use of a polycrystalline titanomagnetite aggregate, which yields diffusion profiles that include a contribution from grain-boundary diffusion (Aragon et al. 1984; Liermann and Ganguly 2002). Therefore in our study we estimate the temperature at which magnetite closed to diffusion by the closure temperature of the Fe–Ti oxide thermometer. During cooling, magnetite and ilmenite re-equilibrate by the  $\text{TiFe}^{2+}\text{Fe}_{-1}^{3+}$  exchange vector. Ferry et al. (1987) obtained Fe–Ti oxide temperatures from the high-grade portion of the contact aureole around Tertiary gabbros and granites on the Isle of Skye. Like the aureole around the Duluth gabbro, the Skye aureole was produced by a shallow gabbroic intrusion and rocks adjacent to it were metamorphosed to extreme temperatures. Pyroxene thermometry from the highest-grade rocks indicate equilibration at temperatures around 1,000°C, whereas Fe–Ti oxide thermometers record temperatures from 650 to 680°C (Ferry et al. 1987). Ferry et al. (1987) maintain that the oxide temperatures are low because they were reset by Fe–Ti interdiffusion on cooling. We suggest that this establishes an empirical closure temperature for Fe-diffusion in magnetite in rapidly cooled terranes (Fig. 8). The empirical closure temperature for magnetite of 650–680°C in the Skye contact aureole is far higher than the ca. 500°C one calculates from the diffusion data of Freer and Hauptman (1978), providing additional evidence that their estimates of diffusion in magnetite are too high.

The probable closure temperature for magnetite is higher than the maximum temperatures attained by samples C–D (Fig. 8), and therefore we do not expect that magnetite in any of these samples re-equilibrated by diffusion during contact metamorphism. On the other hand, sample E did attain temperatures in excess of this 650–680°C and hence potentially may have experienced diffusive resetting. Nevertheless, magnetite can only exchange Fe if there are other minerals that are open to exchange. Because carbonates have reacted out from the iron formation by 500°C, the only likely minerals with which magnetite can exchange are the silicates. Olivine is generally accepted to be the fastest diffusing silicate because it seldom preserves chemical zoning. The diffusion of Fe in olivine therefore places a lower limit on the temperatures at which silicates will close to Fe diffusion. The grain size of olivine from sample E ranges from 1 to 2 mm. Using

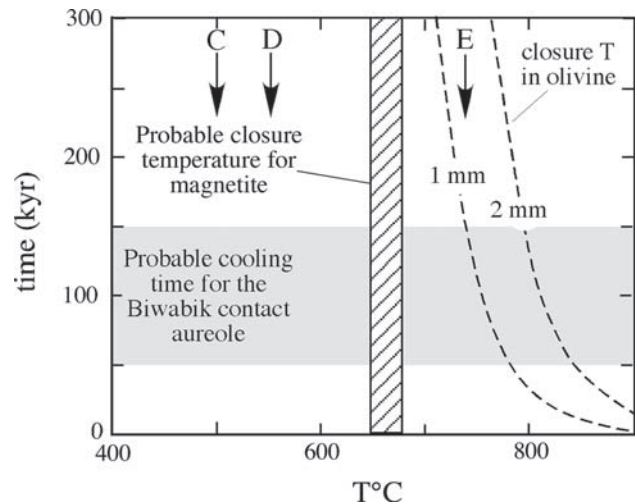
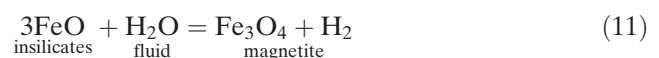


**Fig. 8** Probable closure temperatures for magnetite based upon Fe–Ti oxide thermometry in the Skye contact aureole (Ferry et al. 1987) and for olivine from Mg–Fe interdiffusion in forsteritic olivine (Chakraborty 1997) for grain sizes of 1 and 2 mm. No sample except for sample E attained metamorphic temperatures above the closure  $T$  for magnetite. Valaas and Valley (2005) calculated from oxygen isotope exchange between quartz and magnetite that the high temperature portion of the aureole cooled from 800 to 700°C in 50 ky. Assuming that the thermal pulse in this portion of the aureole lasted between 50 and 150 thousand years (cf. Vallas and Valley 2005), olivine grains of the observed size would be closed to diffusion by 730°C, and therefore oxide-silicate re-equilibration by this mechanism may not have gone to completion in the highest temperatures sample, E

the values for Mg–Fe interdiffusion in forsteritic olivine (Chakraborty 1997) this olivine should be closed to diffusion by 730°C. (Fig. 8). Even olivine one-tenth the size of the grains in sample E would be closed to diffusion in the aureole by around 650°C. These calculations demonstrate that Fe isotopes in magnetite are unlikely to have equilibrated with silicates in any of our samples by process of diffusion.

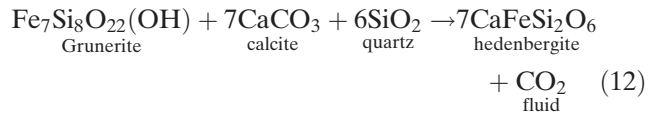
However, magnetite may re-equilibrate at temperatures where it is closed to Fe diffusion if it is involved in metamorphic reactions. Most metamorphic reactions proceed by a dissolution-precipitation process (Carmichael 1969). Minerals participating in a reaction should redistribute their Fe isotopes according to one of the models discussed above (Fig. 7). However, in much of the contact metamorphosed portions of the Biwabik Formation it is unlikely that magnetite participated in the silicate-carbonate reactions during contact metamorphism. The simplest model for the consumption of Fe-silicates in a quartz-excess system to make magnetite is



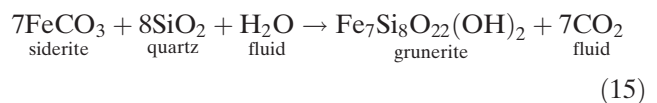
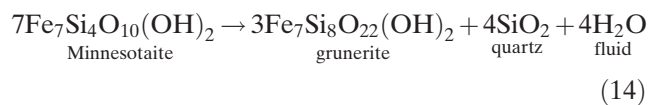
in which one mole of hydrogen is produced for every mole of magnetite. The extent to which this reaction can proceed is governed by the dissociation of water, which itself is a function of oxygen fugacity (Fig. 9). The oxygen fugacity of Biwabik Iron Formation varies between the fayalite–magnetite–quartz buffer (FMQ) (for example, sample E) and the hematite–magnetite buffer (HM) (lying at approximately 5–6 log units above FMQ), represented for example by sample B). At 300°C and at oxygen fugacities of iron formation somewhere between HM and FMQ,  $X(\text{H}_2)$  will be between 0.001 to 0.000001. This means that for every mole of water that moves through the rock, between 0.000001 and 0.001 moles of  $\text{H}_2$  and 0.000001 and 0.001 moles of magnetite may be produced by the oxidation of silicates. This is a negligible amount of magnetite, and we conclude that significant volumes of magnetite are neither formed nor consumed during contact metamorphism. As a result we conclude that over most of the aureole the difference in iron isotope compositions of magnetite and silicates cannot be used as a thermometer (c.f., Johnson et al. 2005a). The one exception may be magnetite and olivine in our highest temperature sample, E. In this sample there is a small amount of Al in the magnetite, which suggests that the magnetite may have incorporated  $\text{FeAl}_2\text{O}_4$  by reaction with amphibole, the only Al-bearing phase.

Rather than involving magnetite, metamorphic silicates form from Fe-bearing carbonates or silicates by reactions that depend upon the composition of the protolith. Hedenbergite-forming reactions depend

upon whether the pyroxene forms in a Fe-bearing silicate or Fe-bearing carbonate layer:



Grunerite-forming reactions also depend upon whether grunerite forms in silicate (reaction 14) or siderite-bearing horizons (reaction 15)



Olivine forms by breakdown of grunerite, which in turn may have ultimately had a carbonate or silicate protolith:

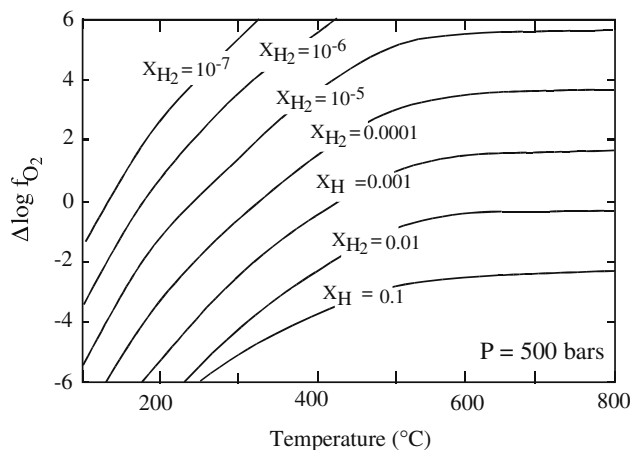
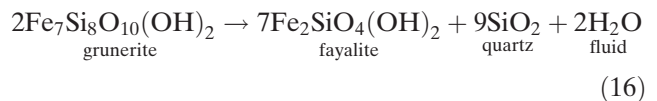


**Fig. 9** Plot of oxygen fugacity (expressed as  $\Delta \log f(\text{O}_2)$  relative to the FMQ buffer) versus temperature at 500 bars, contoured for  $X(\text{H}_2)$ . The oxygen fugacity of Biwabik Iron Formation varies between the FMQ and HM (lying at approximately 5–6 log units above FMQ) buffers. At metamorphic temperatures within this range of oxygen fugacities the oxidation of silicates will cause very little water to dissociate to form  $\text{H}_2$  and magnetite

The important point is that magnetite present in the rocks during contact metamorphism was not involved in the reactions that formed the metamorphic silicates and therefore we cannot assume that it equilibrated isotopically with the silicate minerals. As discussed above, only in the highest temperature sample E is there evidence that magnetite and silicates may have equilibrated with respect to iron isotopes. Even in this sample it is possible that only Fe(II) in magnetite and other minerals equilibrated and that Fe(III) in magnetite was immobile.

The discussion above provides a context in which to interpret the Fe isotope data for metamorphic minerals in contact metamorphosed Biwabik Iron Formation samples.  $\delta^{56}\text{Fe}$  values generally decrease in the order magnetite > silicate  $\geq$  carbonate, which agrees with theoretical predictions from spectroscopic data (e.g., Polyakov and Mineev 2000, Polyakov et al. 2005). The theoretical determination of fractionation factors from spectroscopic data is still in its early stages. Therefore,

whereas the relative sequence of mineral isotope ratios allows valid comparisons, the actual magnitudes of inter-mineral differences have to be used in a semi-quantitative way until  $\beta$ -factors have been validated experimentally. In any case, neither the sequence nor the actual inter-mineral differences between magnetite and Fe-silicate appear to correspond to theoretical predictions. For example, sample E, which was metamorphosed to approximately 730°C, yields  $\Delta^{56}\text{Fe}_{\text{ol-mt}}$  of 0.38‰, sample D, metamorphosed to approximately 550°C yields  $\Delta^{56}\text{Fe}_{\text{gru-mt}}$  of 0.25‰, and sample C metamorphosed to around 500°C yields  $\Delta^{56}\text{Fe}_{\text{cpx-mt}}$  of 0.24‰. In comparison, Polyakov and Mineev (2000, revised by Polyakov et al. (2005) and Polyakov, personal communication) predict that the  $\Delta^{56}\text{Fe}_{\text{ol-mt}}$  at 730°C should be 0.25–0.15‰ (for two different revised magnetite  $\beta$ -factors), whereas  $\Delta^{56}\text{Fe}_{\text{cpx-mt}}$  at 500°C is 0.57–0.4‰. Although discrepancies between the magnitude of predicted and observed Fe isotope fractionations are not uncommon, we suggest that the discrepancy is unrelated to the accuracy of theoretical fractionation factors, but instead reflects the lack of iron equilibration between magnetite and these metamorphic Fe-silicates. We show this in Fig. 10, where measured  $\Delta_{\text{magnetite-silicate}}$  or  $\Delta_{\text{magnetite-carbonate}}$  is plotted as function of metamorphic temperature. Shown too are envelopes for fractionation factors from reduced partition functions (Polyakov and Mineev 2000), where two estimates for the revised magnetite  $\beta$ -factor, determined by both inelastic X-ray scattering, and by new Mössbauer spectroscopic data are used (Polyakov, personal communication). It is obvious from Fig. 10 that at temperatures <500°C the measured  $\Delta^{56}\text{Fe}$  are variable and many measurements do not yield the temperature-dependent isotope fractionation that would be expected if isotopic equilibrium was achieved. Johnson et al. (2003) also have found heavier magnetite than carbonate in Transvaal BIF. As in our study, the Transvaal  $\Delta_{\text{magnetite-carbonate}}$  varied in an inconsistent manner. Our results show that a given mineral can have widely different isotope compositions in adjacent layers (Fig. 5), and suggest the possibility that the Transvaal minerals have not equilibrated but have inherited their precursors compositions

Because magnetite was inert during the formation of the metamorphic silicates, the  $\delta^{56}\text{Fe}$  of these silicates is inherited from precursor Fe-bearing carbonate and silicate minerals. In the cases where only one Fe-bearing mineral reacts to form another (not uncommon in these chemically simple rocks), then the Fe isotopic composition is also transferred unchanged from one mineral to the other, according to model 2 and/or 3 on Fig. 7. For these reasons we interpret the  $\delta^{56}\text{Fe}$  of

metamorphic silicates to reflect the composition of the primary and diagenetic minerals, i.e., either rich in isotopically light carbonate material, or composed of a greater proportion of isotopically heavier silicate and/or oxide component. Of the samples we analyzed, sample D contains the heaviest bulk  $\delta^{56}\text{Fe}$ , which we interpret as inherited from a protolith rich in isotopically heavy silicates and primary oxides. On the other hand, the highest-grade sample, E, has a bulk  $\delta^{56}\text{Fe}$  of approximately 0, which seems to require a greater proportion of isotopically light carbonate in its protolith. A third sample, C, has an intermediate bulk  $\delta^{56}\text{Fe}$ , interpreted as reflecting a protolith with intermediate proportions of heavy and light primary minerals. Not

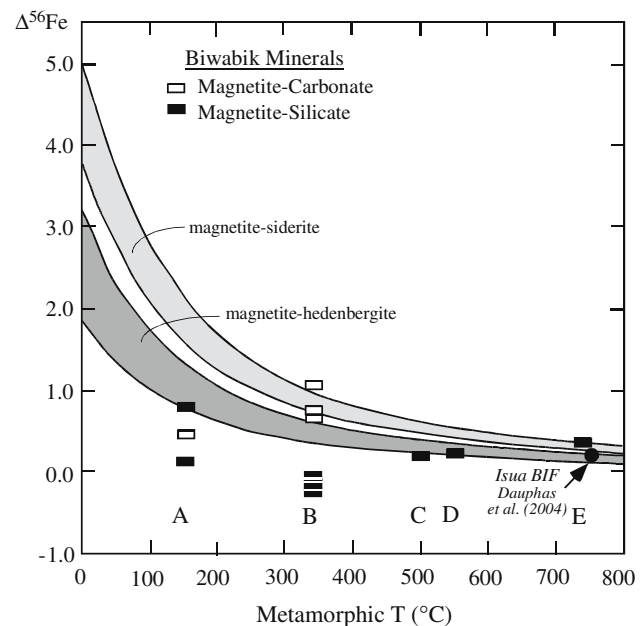


**Fig. 10**  $\Delta^{56}\text{Fe}_{\text{Magnetite-Carbonate}}$  and  $\Delta^{56}\text{Fe}_{\text{Magnetite-Silicate}}$  (Olivine, Chlorite, Hedenbergite, Grunerite, Greenalite) values for Biwabik minerals (Table 2) and theoretic fractionation factors as function of metamorphic temperature. The upper shaded envelope shows fractionation factors for siderite and hedenbergite (Polyakov and Mineev 2000) relative to magnetite, and lower envelope shows the fractionation factors for olivine relative to magnetite (Polyakov et al. 2005, Polyakov, personal communication). In each envelope the upper bound makes use of new reduced partition functions for magnetite as calculated from inelastic X-ray scattering and the lower bound as determined by new Mössbauer spectroscopic data (Polyakov, personal communication). It is important to note that for those mineral pairs that apparently conform to theoretical predictions, the agreement is purely fortuitous because, as discussed in the text, magnetite did not participate in the silicate-forming reactions and temperatures <650°C were insufficient to attain isotopic equilibrium by diffusion. The magnetite–pyroxene pair from regionally metamorphosed BIF studied by Dauphas et al. (2004, closed circle) appears to have equilibrated due to its high temperature and long duration of heating.

only did magnetite not participate in the reactions that form the metamorphic silicates and therefore iron in magnetite did not equilibrate by isotopic exchange during growth of the metamorphic phases. Also at temperatures attained by samples A–D, diffusion of iron within these minerals was too slow to allow for significant iron isotopic equilibration between magnetite and silicate minerals over the short duration of this heating event. As discussed above, it is possible that Fe between silicates and magnetite did exchange by diffusion or reaction in sample E, which reached peak metamorphic temperatures of 725–740°C. Dauphas et al. (2004) measured  $\Delta^{56}\text{Fe}$  of 0.20‰ between magnetite and pyroxene in iron formation metamorphosed to even higher peak temperatures (>750°C) and therefore it is possible that their measured  $\Delta^{56}\text{Fe}$  could also represent isotopic equilibrium (solid circle in Fig. 10). Equilibrium in their samples would have been favoured by the longer heating interval of regional metamorphism.

For these reasons it is not unexpected that some apparent  $\Delta^{56}\text{Fe}$  between magnetite and metamorphic silicates do not conform to theoretical predictions, and we caution against interpreting any of these measured differences in  $\delta^{56}\text{Fe}$  as reflecting isotopic equilibrium during metamorphisms and therefore providing meaningful fractionation factors (cf. Johnson et al. 2003, 2005a).

#### Applicability of results to regional metamorphism

Two important differences between contact and regional metamorphism are that regional metamorphism involves (1) a thermal event of longer duration and (2) a larger scale of fluid flow than does contact metamorphism. The longer duration of regional metamorphism will allow iron isotopes to equilibrate down to lower temperatures. This difference in duration is reflected in the closure temperatures for Fe–Ti oxide thermometry. As noted above, Fe–Ti oxide inter-diffusion closes in contact metamorphism at ca. 650°C (Ferry et al. 1987). In slowly cooled granulite terranes, this closure temperature is between 350 and 500°C (Frost and Chacko 1989). Although the Fe–Ti oxide thermometer is highly uncertain at these low temperatures, these results indicate that whereas Fe-isotopes do not necessarily equilibrate during amphibolite-facies contact metamorphism, they may equilibrate during lower amphibolite or even upper greenschist facies regional metamorphism. In addition, it is possible that extensive fluid flow during regional metamorphism may cause Fe-isotopes to be more readily equilibrated in regionally metamorphosed iron formation than was

documented in the contact-metamorphosed Biwabik Formation. The ability of fluid flow to homogenize a rock depends on the competing kinetics of mineral reaction and fluid flow. Frost and Bucher (1994) showed that at low  $T$ , mineral reactions will be the rate-limiting step and that the crust will consist of isolated pockets of fluid separated by unreacted rock. At temperatures above around 300°C, mineral reactions become faster than fluid flow and in this regime fluids will be consumed in reactions as soon as they encounter a mineral interface. This temperature corresponds to greenschist facies, and is consistent with observations that in prehnite-pumpellyite facies metamorphic rocks are commonly inhomogeneous on a thin-section scale but that they are much more homogenous at greenschist facies. Thus, although large-scale fluid flow may allow equilibration of Fe isotopes in regionally metamorphosed rocks down to lower temperatures than those attained in the contact-metamorphosed Biwabik Iron Formation, weakly metamorphosed rocks should retain small-scale isotopic heterogeneities like those described here, even during regional metamorphism. Regardless of whether minerals have equilibrated during regional metamorphism, these predictions validate the hypotheses of Dauphas et al. (2004). Fe isotope compositions that are characteristic of chemical sedimentation processes are preserved at low grade in the form of large inter-mineral variations, and at high grade in the form of unique bulk rock compositions that are often different than those presented by most igneous and clastic sedimentary rocks. Therefore, our results confirm the suggestion (Johnson et al. 2003; Dauphas et al. (2004; Markl et al. 2006) that Fe isotopes can be used to identify chemical sedimentary or hydrothermal processes in the rock record.

#### Conclusions

The present study of Fe isotopic compositions of minerals in Biwabik Iron Formation has revealed layer-to-layer variations in the  $\delta^{56}\text{Fe}$  of magnetite that are nearly half the total variation observed in magnetite from iron formations of all ages worldwide. These inter-layer variations could be caused by seawater having variable compositions during Fe precipitation into the layers, but are more likely caused by the layers being dominated by certain minerals that incorporate iron according to their specific isotope fractionation factor. Textural evidence from the lowest-grade Biwabik samples reveals that most, if not all, magnetite in the Biwabik Formation is diagenetic, not primary, and that

there was tremendous element mobility during diagenesis. Fluid flow was dominantly layer-parallel, which produced the dramatic layer-to-layer heterogeneities in iron isotopic composition.

The simple chemical composition of iron formation and the large range in  $\delta^{56}\text{Fe}$  of primary and diagenetic silicate, carbonate and oxide minerals might suggest it should be an ideal natural system for verifying theoretical inter-mineral Fe isotope fractionations. However, we have shown that equilibrium Fe isotope fractionation factors cannot be determined from the Biwabik Iron Formation because diagenetic magnetite remained unreactive during metamorphism, and hence did not attain Fe isotopic equilibrium with the metamorphic silicates. Only at the very highest grades, where temperatures were in excess of 700°C may diffusion and mineral reaction have operated to enhance possible Fe isotopic equilibration. For this reason the differences between  $\delta^{56}\text{Fe}$  of magnetite and coexisting metamorphic silicates in rocks metamorphosed to lower peak temperatures do not represent equilibrium fractionation factors, and no temperature information is preserved.

Although iron formation does not record equilibrium inter-mineral Fe isotope fractionations during contact metamorphism or low-grade regional metamorphism, other metasedimentary rock suites may. We suggest, for example, that iron isotopes may be useful in studying metamorphism of graphitic pelitic schists in which magnetite is generally absent. In these rocks, the iron is distributed among pyrite, pyrrhotite and ilmenite and Fe-silicates, and all of these phases may participate in metamorphic reactions (Frost 1992b).

Ultimately it would be desirable to trace the Fe chemistry of the Precambrian oceans using Fe isotopes. Because magnetite is inert during prograde metamorphism. It is potentially a faithful recorder of the earlier environmental conditions in which a sediment formed and was lithified. Therefore Fe isotopes in magnetite–quartz assemblages may preserve information about the Fe chemistry of ancient oceans. However, because most BIF have undergone extensive diagenesis, we suggest that Fe isotopes also can be powerfully employed for tracing movement of Fe during diagenesis. In many clastic sedimentary rocks, iron is precipitated as siderite during methanogenesis (Gautier and Claypool 1984; Raiswell and Fisher 2000). Iron isotopes may reveal whether this iron is locally derived or far-traveled. Together with C isotopic data, they may be useful in determining the role of methanogenesis during the fractionation of iron isotopes.

## References

- Anbar AD, Jarzecki AA, Spiro TG (2005) Theoretical investigation of iron isotope fractionation between  $\text{Fe}(\text{H}_2\text{O})^{3+6}$  and  $\text{Fe}(\text{H}_2\text{O})^{2+6}$ : implications for iron stable isotope geochemistry. *Geochimica Cosmochimica Acta* 69:825–837
- Andersen DJ, Lindsley DH, Davidson PM (1993) QUILF: a Pascal program to assess equilibria among Fe–Mg–Ti oxides, pyroxenes, olivine, and quartz. *Comput Geosci* 19:1333–1350
- Andrews MS, Ripley EM (1989) Mass transfer and sulfur fixation in the contact aureole of the Duluth Complex, Dunka River Cu–Ni deposit, Minnesota. *Can Mineral* 27:293–310
- Aragon R, McCallister RH, Harrison HR (1984) Cation diffusion in titanomagnetites. *Contrib Mineral Petrol* 85:174–185
- Arnold GL, Weyer S, Anbar AD (2004) Fe isotope variations in natural materials measured using high resolution multiple collector ICPMS. *Anal Chem* 76:322–327
- Barghoorn ES, Tyler SA (1965) Microorganisms from the Gunflint Chert. *Science* 147:563–577
- Beard BL, Johnson CM (2004) Inter-mineral Fe isotope variations in mantle-derived rocks and implications for the Fe geochemical cycle. *Geochimica et Cosmochimica Acta* 68:4727–4743
- Beard BL, Johnson CM, Skulan JL, Nealson KH, Cox L, Sun H (2003) Application of Fe isotopes to tracing the geochemical and biological cycling of Fe. *Chemical Geol* 195:87–117
- Berman RG (1988) Internally-consistent thermodynamic data for minerals in the system  $\text{Na}_2\text{O}$ – $\text{K}_2\text{O}$ – $\text{CaO}$ – $\text{MgO}$ – $\text{FeO}$ – $\text{Fe}_2\text{O}_3$ – $\text{Al}_2\text{O}_3$ – $\text{SiO}_2$ – $\text{TiO}_2$ – $\text{H}_2\text{O}$ – $\text{CO}_2$ . *J Petrol* 29:445–522
- Bonnichsen B (1969) Metamorphic pyroxenes and amphiboles in the Biwabik Iron Formation, Dunka River area, Minnesota. *Mineral Soc Am Spec Pap* 2:217–239
- Bonnichsen B (1975) Geology of the Biwabik Iron Formation, Dunka River area, Minnesota. *Econ Geol* 70:319–340
- Brantley SL, Liermann LJ, Gwynn RL, Anbar A, Icopini GA, Barling J (2004) Fe isotopic fractionation during mineral dissolution with and without bacteria. *Geochimica et Cosmochimica Acta* 68:3189–3204
- Bullen TD, White AF, Childs CW, Vivit DV, Schulz MS (2001) A demonstration of significant abiotic iron isotope fractionation in nature. *Geology* 29:699–702
- Carmichael DM (1969) On the mechanism of prograde metamorphic reactions in quartz-bearing pelitic rocks. *Contrib Mineral Petrol* 20:244–267
- Chakraborty S (1997) rates and mechanisms of Fe–Mg interdiffusion in olivine at 980–1300°C. *J Geophys Res* 102:12317–12331
- Chang SBR, Stolz JF, Kirschvink JL, Awramik SM (1989) Biogenic magnetite in stromatolites II. Occurrences in ancient sedimentary environments. *Precambrian Res* 43:305–315
- Chu N-C, Johnson CM, Beard BL, German CR, Nesbitt RW, Usui A (2003) Secular Fe isotope variations in the central Pacific Ocean. *Geochimica et Cosmochimica Acta* 67:A66
- Clayton RN, Keefer SW (1991) O isotope thermometer calibration. In Taylor HP, O'Neil JR, Kaplan IR (eds) *Stable isotope geochemistry: a tribute to Samuel Epstein*. Geological Society Special Publication 3:3–10
- Dauphas N, van Zuilen M, Wadhwa M, Davis AM, Marty B, Janney PE (2004) Clues from Fe isotope variations on the origin of early Archean BIFs from Greenland. *Science* 306:2077–2080
- Evans BW, Ghiorso MS (1995) Thermodynamics and petrology of cummingtonite. *Am Mineral* 80:649–663

- Ferry JM, Mutti LJ, Zuccala GJ (1987) Contact metamorphism/hydrothermal alteration of Tertiary basalts from the Isle of Skye, northwest Scotland. *Contrib Mineral Petrol* 95:166–181
- Floran RJ, Papike JJ (1975) Petrology of the low-grade rocks of the Gunflint Iron-Formation, Ontario-Minnesota. *Geol Soc Am Bull* 86:1169–1190
- Floran RJ, Papike JJ (1978) Mineralogy and petrology of the Gunflint Iron Formation, Minnesota-Ontario: correlation of compositional and assemblage variations at low to moderate grade. *J Petrol* 19:215–288
- Fralick P, Davis DW, Kissin SA (2002) The age of the Gunflint Formation, Ontario, Canada: single zircon U-Pb age determinations from reworked volcanic ash. *Can J Earth Sci* 39:1085–1091
- Freer R, Hauptman Z (1978) An experimental study of magnetite-titanomagnetite interdiffusion. *Phys Earth Planet Inter* 16:223–231
- French BM (1968) Progressive contact metamorphism of the Biwabik Iron-Formation, Mesabi Range, Minnesota. *Minnesota Geological Survey Bulletin* 45:103
- Frost BR (1979) Metamorphism of Iron-Formation: parageneses in the system Fe–Si–C–O–H. *Econ Geol* 74:775–785
- Frost BR (1992a) Introduction to oxygen fugacity and its petrologic importance. *Rev Mineral* 25:1–9
- Frost BR (1992b) Magnetic petrology: factors that control the occurrence of magnetite in crustal rocks. *Rev Mineral* 25:489–509
- Frost BR, Chacko T (1989) The granulite uncertainty principle: limitations on thermobarometry in granulites. *J Geol* 97:435–450
- Frost BR, Bucher K (1994) Is water responsible for geophysical anomalies in the deep continental crust? A petrological perspective. *Tectonophysics* 231:293–309
- Frost BR, Lindsley DH, Andersen DJ (1988) Fe–Ti oxide-silicate equilibria: assemblages with fayalitic olivine. *Am Mineral* 73:727–740
- Gautier DL, Claypool GE (1984) Interpretation of metanic diagenesis in ancient sediments by analogy with processes in modern diagenetic environments. *Am Assoc Petrol Geol Memoir* 37:111–123
- Gilletti B (1986) Diffusion effects on oxygen isotope temperatures of slowly cooled igneous and metamorphic rocks. *Earth Planet Sci Lett* 77:218–228
- Graham S, Pearson N, Jackson S, Griffin W, O'Reilly SY (2004) Tracing Cu and Fe from source to porphyry: in situ determination of Cu and Fe isotope ratios in sulfides from the Graserg Cu–Au deposit. *Chem Geol* 207:147–169
- Gundersen JN, Schwartz GM (1962) The geology of the metamorphosed Biwabik Iron-Formation, eastern Mesabi district, Minnesota. *Minnesota Geological Survey Bulletin* 43:139
- Han T-M (1978) Microstructures of magnetite as guides to its origin in some Precambrian iron-formations. *Fortschritte der Mineralogie* 56:105–142
- James HL, Dutton CE, Pettijohn FJ, Weir KL (1968) Geology and ore deposits of the Iron River-Crystal Falls District, Iron County, Michigan. *US Geological Survey Professional Paper* 570, 134
- Johnson CM, Beard BL, Beukes NJ, Klein C, O'Leary JM (2003) Ancient geochemical cycling in the earth as inferred from Fe isotope studies of banded iron formations from the Transvaal Craton. *Contrib Mineral Petrol* 144:523–547
- Johnson CM, Beard B, Valley J, Valaas E (2005a) Preservation of Fe isotope proxies in the rock record. *EOS abstract* PP43B-0689
- Johnson CM, Roden EE, Welch SA, Beard BL (2005b) Experimental constraints on Fe isotope fractionation during magnetite and Fe carbonate formation coupled to dissimilatory hydrous ferric oxide reduction. *Geochimica et Cosmochimica Acta* 69:963–993
- Juneau P (1979) Origin and petrology of iron silicate-rich bodies in the Biwabik Iron Formation, Minnesota. Unpublished MS thesis, University of Minnesota-Duluth, 209
- Klein C (2005) Some Precambrian banded iron-formations (BIFs) from around the world: their age, geologic setting, mineralogy, metamorphism, geochemistry, and origin. *Am Mineral* 90:1473–1499
- Knoll AH, Barghoorn ES, Awramik SM (1978) New microorganisms from the Aphebian Gunflint iron formation, Ontario. *J Paleontol* 52:976–992
- Konhauser KO (1998) Diversity of bacterial iron mineralization. *Earth Sci Rev* 43:91–12
- Konhauser KO, Hamade T, Raiswell R, Morris RC, Ferris FC, Southam G, Canfield DE (2002) Could bacteria have formed the Precambrian banded iron formations? *Geology* 30:1079–1082
- LaBerge GL (1964) Development of magnetite in iron-formations of the Lake Superior region. *Econ Geol* 59:1313–1342
- Lanier WP (1989) Interstitial and peloidal microfossils from the 2.0 Ga Gunflint Formation: implications for the paleoecology of the Gunflint stromatolites. *Precambrian Res* 45:291–318
- Lattard D, Evans BW (1992) New experiments on the stability of grunerite. *Eur J Mineral* 4:219–238
- Liermann HP, Ganguly J (2002) Diffusion kinetics of Fe<sup>2+</sup> and Mg in aluminous spinel: experimental determination and applications. *Geochimica et Cosmochimica Acta* 66:2903–2913
- Lovley D (1990) Magnetite formation during microbial dissimilatory iron reduction. In: Frankel RB, Blakemore RP (eds) *Iron biominerals*. Plenum Press, New York, pp 151–166
- Lovley DR, Stolz JF, Nord GLJ, Phillips JP (1987) Anaerobic production of magnetite by a dissimilatory iron-reducing microorganism. *Nature* 330:252–254
- Markl G, von Blanckenburg F, Wagner T (2006) Iron isotope fractionation during hydrothermal ore deposition and alteration. *Geochim et Cosmochim Acta* 70: 3011–3030
- Matthews A, Morgans-Bell HS, Emmanuel S, Jenkyns HC, Erel Y, Halicz L (2004) Controls on iron-isotope fractionation in organic-rich sediments (Kimmeridge Clay, Upper Jurassic, southern England). *Geochimica et Cosmochimica Acta* 68:3107–3123
- Morey GB (1992) Chemical composition of the eastern Biwabik Iron-formation (Early Proterozoic), Mesabi Range, Minnesota. *Econ Geol* 87:1649–1658
- Morey GB, Papike JJ, Smith RW, Weiblen PW (1972) Observations on the contact metamorphism of the Biwabik Iron Formation, East Mesabi district, Minnesota. *Geol Soc Am Memoir* 135:225–263
- Perry EC, Tan FC, Morey GB (1973) Geology and stable isotope geochemistry of the Biwabik Iron Formation, northern Minnesota. *Econ Geol* 68:1110–1125
- Poitras F, Frey R (2005) Heavy iron isotope composition of granites determined by high resolution MC-ICP-MS. *Chem Geol* 222:132–147
- Poitras F, Halliday AN, Lee DC, Lévassieur S, Teutsch N (2004) Iron isotope differences between Earth, Moon, Mars and Vesta as possible records of contrasted accretion mechanisms. *Earth Planet Sci Lett* 223:253–266
- Polyakov VB, Mineev SD (2000) The use of Mössbauer spectroscopy in stable isotope geochemistry. *Geochimica et Cosmochimica Acta* 64:849–865

- Polyakov VB, Mineev SD, Clayton RN (2005) Iron and tin isotope equilibrium fractionation factors from Mössbauer and synchrotron radiation data. *Geochimica et Cosmochimica Acta* 69:A210
- Raiswell R, Fisher QJ (2000) Mudrock-hosted carbonate concretions: a review of growth mechanisms and their influence on chemical and isotopic composition. *J Geol Soc (Lond)* 157:239–251
- Rasmussen MG, Evans BW, Kuehner SM (1998) Low temperature fayalite, greenalite, and minnesotaite from the Overlook gold deposit, Washington: phase relations in the system FeO-SiO<sub>2</sub>-H<sub>2</sub>O. *Can Mineral* 36:147–162
- Rouxel OJ, Bekker A, Edwards KJ (2005) Iron isotope constraints on the Archean and Paleoproterozoic ocean redox state. *Science* 307:1088–1091
- Schauble EA (2004) Applying stable isotope fractionation theory to new systems. *Rev Mineral Geochem* 55:65–111
- Schauble EA, Rossmann GR, Taylor HP (2001) Theoretical estimates of equilibrium Fe-isotope fractionations from vibrational spectroscopy. *Geochimica et Cosmochimica Acta* 65:2487–2497
- Schoenberg R, von Blanckenburg F (2005) An assessment of the accuracy of stable Fe isotope ratio measurements on samples with organic and inorganic matrices by high-resolution multicollector ICP-MS. *Int J Mass Spectrom* 242:257–272
- Schoenberg R, Kamber BS, von Blanckenburg F (2005) Comparative stable Fe isotope systematics of terrestrial and meteoritic materials. *Geochimica et Cosmochimica Acta* 69:A398
- Schuessler J, Schoenberg R, Behrens H, von Blanckenburg F (2005) Experimental calibration of the Fe isotope fractionation between pyrrhotite and silicate melt. *Geochimica et Cosmochimica Acta* 69:A211
- Sharma M, Polizzotto M, Anbar AD (2001) Iron isotopes in hot springs along the Juan de Fuca Ridge. *Earth Planet Sci Lett* 194:39–51
- Simonson BM (1985) Sedimentological constraints on the origins of Precambrian iron-formations. *Geol Soc Am Bull* 96:244–252
- Simonson BM (1987) Early silica cementation and subsequent diagenesis in arenites from four Early Proterozoic iron formations of North America. *J Sediment Petrol* 57:494–511
- Simmons EC, Lindsley DH, Papike JJ (1974) Phase relations and crystallization sequence in a contact-metamorphosed rock from the Gunflint Iron Formation, Minnesota. *J Petrol* 15:539–565
- Skulan JL, Beard BL, Johnson CJ (2002) Kinetic and equilibrium Fe isotope fractionation between aqueous Fe(III) and hematite. *Geochimica et Cosmochimica Acta* 66:2995–3015
- Valaas EP, Valley JW (2005) Oxygen isotope speedometry in the Biwabik iron-formation. *Geochimica et Cosmochimica Acta* 69:A399
- Welch SA, Beard BL, Johnson CM, Braterman PS (2003) Kinetic and equilibrium Fe isotope fractionation between aqueous Fe(II) and Fe(III). *Geochimica et Cosmochimica Acta* 67:4231–4250
- Weyer S, Schwieters J (2003) High precision Fe isotope measurements with high mass resolution MC-ICPMS. *Int J Mass Spectrom* 226:355–368
- Weyer S, Anbar AD, Brey GP, Münker C, Mezger K, Woodland AB (2005) Iron isotope fractionation during planetary differentiation. *Earth Planet Sci Lett* 240:251–264
- Wiesli RA, Beard BL, Johnson CM (2004) Experimental determination of Fe isotope fractionation between aqueous Fe(II), siderite and “green rust” in abiotic systems. *Chem Geol* 211:343–362
- Williams HM, McCammon CA, Peslier AH, Halliday AN, Teutsch N, Levasseur S, Burg J-P (2004) Iron isotope fractionation and the oxygen fugacity of the mantle. *Science* 304:1656–1659
- Winter BL, Knauth LP (1992) Stable isotope geochemistry of cherts and carbonates from the 2.0 Ga Gunflint Iron Formation: implications for the depositional setting, and the effects of diagenesis and metamorphism. *Precambrian Res* 59:283–313
- Yamaguchi KE, Johnson CM, Beard BL, Ohmoto H (2005) Biogeochemical cycling of iron in the Archean-Paleoproterozoic Earth: constraints from iron isotope variations in sedimentary rocks from the Kaapvaal and Pilbara cratons. *Chem Geol* 218:135–169
- Zhu XK, O’Nions RK, Guo Y, Reynolds BC (2000) Secular variation of iron isotopes in North Atlantic Deep Water. *Science* 287:2000–2002
- Zhu XK, Guo Y, Williams RJP, O’Nions RK, Matthews A, Belshaw NS, Canters GW, de Waal EC, Weser U, Burgess BK, Salvato B, (2002) Mass fractionation processes of transition metal isotopes. *Earth Planet Sci Lett* 200:47–62